Freeze Casting of Aqueous PAA-Stabilized Carbon Nanotube-Al_2O_3 Suspensions

by

Christopher S. Kessler

Thesis submitted to the faculty of the
Virginia Polytechnic Institute and State University
in partial fulfillment of the requirements for the degree of

Master of Science

in

Materials Science and Engineering

APPROVED:

Dr. Kathy Lu, Chair
Dr. Kathryn V. Logan
Dr. David Clark

July 7, 2006

Blacksburg, Virginia

Keywords: colloidal, dispersion, nano, nanopowder, carbon nanotubes, rheology, freeze casting, bulk nanomaterials, dispersant, adsorption, PAA, PMAA, sintering, Al_2O_3

Freeze Casting of Aqueous PAA-Stabilized Carbon Nanotube-Al_2O_3 Suspensions

Christopher S. Kessler

ABSTRACT

Freeze casting is a colloidal processing technique that shows great promise for development of nanostructured materials. A ceramic nanopowder is dispersed with a polymer in water, under carefully controlled pH. The suspension is cast into a suitable mold and frozen, then de-molded and exposed to a vacuum to sublimate and remove the water. Polymer adsorption and rheology were studied to optimize and characterize a colloidal suspension of a 38 nm Al_2O_3 powder. The dispersant, dispersant amount, pH and solids loading were examined to determine the best conditions for freeze casting. Based on adsorption and viscosity data, optimal conditions for freeze casting were found with Poly(acrylic acid) (PAA) dispersant, at 2.00 wt% (of Al_2O_3), pH of 9.5, and a solids loading of 40 vol%. Carbon nanotubes (CNTs) were added to that suspension in increments of 0.14, 0.28, 0.53, 1.30 and 2.60 vol%. The viscosity increased dramatically upon addition of 1.30 vol% CNTs. The colloidal CNT-Al_2O_3 suspension was successfully freeze cast and the microstructure showed a very smooth fracture surface. It was determined that upon resting, the suspension undergoes a physical change which must be completed to obtain advantageous microstructure. Freeze cast Al_2O_3 discs with and without CNTs were measured using a concentric ring test, with strengths on the order of one MPa. The freeze cast sample was successfully debinded, but the heating profile attempted was not effective in obtaining full density.

ACKNOWLEDGEMENTS

I would like to extend my deepest thanks to my advisor, Dr. Kathy Lu, for her help and guidance. Without your patience and wisdom, this project would never have come to fruition.

To my committee members, Dr. David Clark and Dr. Kathryn Logan, thank you for providing me with valuable insight into this project, as well as in the broader scope of materials science.

The Lu research group has provided me with assistance and companionship in and out of the lab, for which I am thankful.

Dr. Brian Love, Dr. Gary Pickrell, Dr. Jeff Schultz, and many other faculty in the MSE Department have graciously allowed me to use their equipment and lab space while working on this project, as well as answering many questions. Your help is greatly appreciated.

To David Berry, who has helped me and so many others in our department countless times, I can only say that we will be lost without you.

Finally, I would like to thank my family for making me the man I am today.

TABLE OF CONTENTS

LIST OF FIGURES

LIST OF EQUATIONS

SYMBOL DEFINITIONS:

a	particle radius
b	proportionality constant
c	power law exponent
D	diameter of disc
D_L	diameter of load ring
D_S	diameter of support ring
F	breaking load
G*	complex shear modulus
G'	storage modululs
G"	loss modulus
h	disc thickness
M_w	molecular weight
n	power law exponent
R_H	size of random polymer coil
δ	adsorbed layer thickness
η	viscosity
η_0	intrinsic viscosity
η_r	relative viscosity
γ	shear strain
$\dot{\gamma}$	shear strain rate
τ	shear stess
Γ	polymer adsorption amount
φ	volume fraction of suspended particles
φ_m	maximum volume fraction of suspended particles
ϕ	solids loading
ϕ_{eff}	effective solids loading,
ν	Poisson's ratio

LIST OF TABLES

Chapter 1. Nanomaterials Overview

ABSTRACT

Nanomaterials are one of the most important research areas in the last ten years, with broad application in almost all industries. Carbon nanotubes (CNTs) offer an interesting opportunity as a composite reinforcement phase because of several unique properties. Bulk nanomaterials have not been explored to their full advantage. Bulk nanomaterials have been hampered with the difficulties of maintaining ultrafine features while processing real samples, making colloidal processing necessary. Colloidal theories and techniques are discussed in detail. Freeze casting is one colloidal processing technique that might be used to create a bulk nanomaterial-carbon nanotube composite material. The challenges are to maintain a homogeneous nanostructure in a fully dense ceramic while imparting the benefit of carbon nanotubes.

1.1Why are nanomaterials important?

1.1A What are nanomaterials?

A nanomaterial is any structure which contains at least one dimension of size 100 nm or less. By this definition, many different nanomaterials have been constructed in recent years. Thin epitaxial films, nano-sized powders, and quantum dots have all been engineered from any number of metal, ceramic, and polymer systems.[1] Thin films can provide an excellent chemical barrier or impart desirable electrical properties at a low material and labor cost. Quantum dots have seen use for in-vivo medical diagnostic procedures, which were impossible even 20 years ago. Extremely thin nanofilms of material can provide chemical protection or reactivity for a surface at minimal costs, and

powders with nano-size particles allow certain processing advantages, and make it easier to create bulk nanomaterials. Bulk nanomaterials refer to a macro-scale part that is composed of nanostructures.

1.1B What are carbon nanotubes and their application?

Carbon nanotubes (CNTs) are a unique material that has shown outstanding potential for a number of high-strength and specialty applications. Since their discovery in 1991,[2] CNTs have generated a tremendous research effort to try to understand, characterize and utilize these materials. The CNTs can be described as graphitic carbon, rolled into a tube, either a single layer (Single-wall Carbon Nanotube, SWCNT) or multiple concentric layers (Multi-wall Carbon Nanotube, MWCNT).

The research effort to understand CNTs is driven by their unique properties. There are several different configurations of carbon nanotubes, and the CNT can be either metallic or semiconducting.[3,4] CNTs have been shown to be outstanding field emitters,[5] have highly anisotropic electrical properties,[6] and can even be used to create unique structures of metals through capillary forces.[7] Strengths in the 100 GPa range, and elastic moduli in the TPa range have been measured and calculated for CNTs.[8, 9] Because of the nanoscopic and fibrillar nature of CNTs, the greatest mechanical advantage may be gained by use as a fiber reinforcement in composite materials. A high aspect ratio molecule makes a good reinforcement phase because less is needed to make a percolated structure compared with spherical particles, and because it can be oriented preferentially, advantageous nanostructures never before possible can be created.[10] CNT-Polymer composites have been created to enhance the strength of epoxy and poly(methyl methacrylate),[11,12] and to replace other additives, such as carbon black, used to change the

electrical conductivity in many other polymers.[13] Special challenges are encountered when CNTs are incorporated into a ceramic matrix, which will be discussed later.

1.1C What are the unique properties of bulk nanomaterials?

Materials with nano-size grains offer high strength-to-weight ratios, lower hardness, and better elastic modulus than coarser-grained materials. Ceramics made from nanoparticles can be sintered at much lower temperatures and shorter time, saving money, and can be made into dense parts with nano-sized grains or nanostructures. Nanocrystalline ceramics have been shown to be superplastic, having very high deformation before fracture. The high plasticity is possible because of grain boundary sliding during deformation. Nanocrystalline ceramics have also been shown to have very high fracture toughness, as high as 16-17 MPa $m^{1/2}$.[14]

1.1D What are the processing challenges?

Usually at the temperatures necessary to densify ceramics, grain growth is in effect. This grain growth tends to destroy nanostructures. The challenge presented to the ceramic engineer is to develop functional nanostructures in the bulk material which will last. Additionally, the high specific surface area of nano-size powders causes great difficulty during forming due to frictional forces. Traditional methods of compaction such as uniaxial pressing cannot generate enough force to overcome friction from nanopowders, and yield green compacts of low density, unsuitable for densification. For nano-size powders the surface chemistry becomes critically important because a far greater percentage of the material lies on the surface. Additionally, increased capillary force due to decrease in pore size means drying can be especially problematic for nanopowders processed with water.[15]

1.2 What are the potential problems associated with nanomaterial processing?

Because of extremely high specific surface area, nanopowders are more susceptible to agglomeration than micron-sized particles. The undesired agglomeration can be created during synthesis of the powders, during drying, or even during storage of the powder. One way to prevent agglomeration of ceramic nanopowders is to sheath the individual particles in a protective coating. In some cases, thin adsorbed layers of polymer have been successfully applied to powder to prevent agglomeration.

Forming of ceramic nanopowders has caused considerable difficulty in the past. Uniaxial pressing of the powders into a green compact is not effective with these types of materials. Smaller particle size leads to huge interfacial and point contact between particles, causing significant resistance to compaction due to friction. In order to overcome this effect, higher stresses are usually used, but the conventional press often cannot deliver the high stress needed and the dies can not withstand the high pressure. Higher stress also results in higher residual stresses in the green compact, creating defects, density gradients, and macroscopic cracks. Another method to address agglomeration issues is to employ colloidal processing of nanopowders, which is discussed at length in section 1.3.

Sintering of green bodies to obtain a bulk nanostructured material is also problematic. Sintering is a diffusional process. There are different types of diffusion, which can cause either densification or grain coarsening for a particle compact. The grain growth mechanism occurs at relatively low temperatures. As temperature increases, both lattice and grain boundary diffusion occur. Grain growth mechanisms are still active as the densification mechanism begins, so the heating rates leading to the

sintering temperature should be fast to favor densification more. For nanopowder compacts the challenge of sintering is to densify the structure and eliminate porosity while avoiding grain growth.

Porosity may also have a significant effect on sintering behavior. After the porosity is isolated, any gas present in those pores is trapped, and will tend to prevent further densification. To prevent gas from remaining in the sintered ceramic, vacuum may be applied. Modeling of the closing of pores is very complex. For example, although grain growth and densification are competing phenomena, in the ZrO_2 –3 mol% Y_2O_3 system, the porosity hinders densification, but not grain growth. For this system, fully dense nanocrystalline ceramics can be obtained by minimizing porosity before sintering.

Phase changes present a challenge to sintering as well. Many ceramic systems such as Al_2O_3 and TiO_2 undergo a phase change at temperatures needed for sintering. Once the new phase has nucleated, the grains may grow to a very large size. Engineers often use powders of the high-temperature phase (α-Al_2O_3 or rutile in TiO_2) in order to prevent a phase change during sintering.

To offset the propensity of grain growth during heating, a number of techniques may be employed. By adding a secondary element that forms a grain boundary phase, grain growth can be hindered. Grains are free to move closer, and grain boundary diffusion occurs; however the grain boundaries are pinned by small amounts of the impurity phase, effectively controlling grain size. Composite materials often have processing advantages over single phases. By adding fibers of a different material, for

example, grains are prevented from growing because the fiber material is not soluble in the lattice.

1.3 Colloidal dispersions

In this section, colloidal dispersion will be addressed from the following aspects: 1) what are the interparticle forces that cause powders to agglomerate, 2) how are these forces overcome, 3) what are the complications arriving in these added processing steps?

1.3A Interparticle force

Like numerous other species, ceramic particles exhibit a net electrodynamic attraction to one another, commonly referred to as van der Waals Forces. This attraction is the result of oscillating dipoles. In 1934, London described the atomic attraction between two transitory dipoles, which are the most important of the van der Waals forces for colloidal processing considerations.[16] While it is true that van der Waals forces between individual atoms are very small, and of short range, it must be considered that every atom is attracted to every other atom in every particle in the dispersion. Thus the net force of the interaction between two particles can be considered to have effective range on the order of nanometers.[17]

The available free ions in the liquid have a strong effect on the double layer strength and charge. For a low pH, net surface charge is negative. For a high pH, net surface charge is positive. Cesarano and Aksay found the zero point of charge (zpc) of α-Al_2O_3 to be 8.7 in water.[18] When a particle immersed in a liquid carries a net surface charge, ions in the liquid will gather around that particle. This layer of oppositely-charged particle and ions is called the double layer. A positively charged particle in water will have a shortage of cations, and extra anions surrounding it. This charge effect

will generate both electrical and osmotic potential in the liquid, which is repulsive between particles.[19]

The surface potential can be calculated easily, however, the diffuse double layer does not start at the charged surface, but rather from a short distance away from it, denoted by the Stern plane. For the purposes of real measurements, zeta potential is used to approximate the potential in the Stern plane. Zeta potential is the potential at a distance from the surface that the solvent molecules can move toward the surface.

1.3B Stabilization mechanisms

As mentioned previously, the presence of ions in solution can counteract the attractive forces between particles. This ion-related stabilizing force is called electrostatic stabilization. The pH of the solution can be adjusted according to the surface charge of the ceramic particles. For this stabilization mechanism to be effective, the surface charge of the particles must be strong enough to cause a significant difference in local ion concentration around the particles, and the diffuse double layer must be sufficiently large to prevent van der Waals attractions from becoming strong. The surface charge can be measured via zeta potential, while adjusting the pH of the solution controls the ionic concentration, and thus the diffuse double layer thickness.

The unique ionic properties of water allow many methods for overcoming the problematic interparticle attraction inherent in most ceramics. A polymer species can be added to the suspension, which can adsorb onto the surface of the particles. The polymer chains extend into the liquid, and physically repel one another. This method of stabilizing a colloidal dispersion is known as steric stabilization. The effectiveness of steric dispersion is dependent upon several factors. The polymer species must adsorb to

the ceramic particles in suspension. Adsorption is dependent on the type of polymer (homopolymer, diblock copolymer, short-chain functional polymer).[20] Also, the polymer can take several configurations upon adsorption, as shown in figure 1. In the train configuration, the polymer is adsorbed flatly onto the surface of the particle. In the tail configuration, the polymer has very little contact with the particle, and extends into the liquid. The loop configuration is a combination of train and tail behavior. Usually, the tail adsorption is preferred to provide the micellar structure shown in figure 1, which keeps the oxide particles apart and promotes good dispersion.

Usually adsorption is favored by a difference in net surface charge, such as a positive charge for Al_2O_3 and a negative charge for poly(methacrylic acid) (PMAA). Cesarano showed that addition of an anionic polymer dispersant is a simple way to obtain well-dispersed, electrosterically-stabilized aqueous slurry with greater than 50% solids loading. The adsorbed polymer changes the net surface charge of the system, and polymer strands repel one another because of the potential generated.[21] It is important to note that the high surface charge of the polymer species means that electrostatic forces are strong. Hence, this method of colloid stabilization is commonly referred to as "electrosteric." The adsorbed polymer must be thick enough to prevent close contact, counteracting the weak van der Waals forces. There must be enough polymer present to provide complete coverage of the ceramic particles. Incomplete coverage will cause polymer strands to "bridge" the gap between particles, resulting in bridging flocculation.[22]

Since the dispersion contribution of adsorbed polyelectrolytes is dependent on electrostatic as well as steric mechanisms, pH must be controlled to prevent imparting an

attractive force between particles. Singh *et al.* found that use of ammonium poly(methacrylic acid) (NH_4-PMAA, Darvan C) as a dispersant shifts zpc of the system from 9.14 to 5.65. Surface charge of the oxide particle attracts negative ions from the polymer. Surface charge of the polymer dominates, and a higher pH will result in a more dispersed solution.[23] The net charge of the system is reversed due to the adsorption of the negatively-charged polymer.

1.3C What are problems associated with processing?

Although great success has been achieved in creating stable suspensions with high solids loading using PMAA for electrosteric stabilization, a delicate balance must be maintained in the amount of dispersant in the system. Too little polymer will cause bridging flocculation to occur. As dispersant concentration is increased, the surface coverage of the polymer on the oxide is increased to a saturation, or complete coverage of

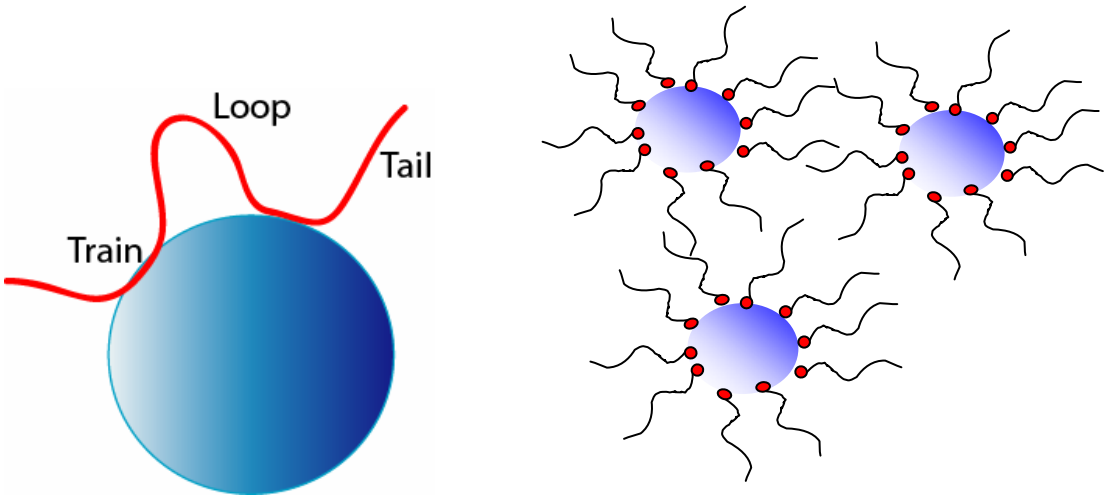

Figure 1. a) Schematic of polymer chain (red) adsorbed onto an oxide particle (blue). b) adsorbed polymer prevents agglomeration in steric stabilization.

the surface. At saturation, steric stabilization becomes effective. The pH of the system must be adjusted to attain a net electrostatic repulsion, and not an attraction. As electrolyte dispersant concentration is increased further, the non-adsorbed free polymer will tend to deflocculate the suspension, and steric stabilization is dominant even at pH that would apply electrostatic stabilization.[24] The amount of adsorbed polymer, **Γ,** needed to attain saturation is dependent on the particle size of the ceramic powder, the polymer dispersant used, and the solids loading level.

Adsorption of the polymer is a kinetic process, and may not occur to saturation. The polymer adsorption is also dependent upon both concentration and pH, and for an ionic polymer, can be described by the van der Schee model. In this model, both electrical charge and surface forces are considered to generate an adsorption lattice. For a charged polymer, loop and tail formation is suppressed in favor of more train adsorption.[25] Adjusting pH from a value of 8.2 to 9.8 causes a decrease of the saturation level of adsorption of PMAA in α-Al_2O_3 by a factor of two. Adsorption of the negatively-charged polymer on the positively-charged oxide occurs spontaneously, however, as the adsorption of polymer increases, the net charge of the system decreases, and a counter ion cloud develops as a barrier to further adsorption. An excess of electrolyte is therefore needed to attain saturation adsorption at pH values above the zero point of charge (for a negative net-charge system).

Cesarano, Aksay, and Bleier, among others, have shown that the viscosity of polyelectrolyte-stabilized aqueous slurries is highly dependent upon pH, and that viscosity is minimized at pH value near 8.8. (Though this was near the original zpc for Al_2O_3 in water, surface-adsorbed dispersant changes the zpc to acidic values). At pH

higher than zpc, excess polyelectrolyte hinders steric stabilization. Although adsorption favors the "high affinity" model described by van der Schee, dissociation of PMAA (Darvan C) increases with increasing pH. At acidic pH, RCOOH is favored over RCOO- resulting in adsorption less than saturation. As net charge of the system decreases through higher amounts of polymer (adsorbed), the polymer will extend fewer functional groups into solution, decreasing steric stabilization. Higher ionic content in the solution also decreases the electrostatic contribution of the polymer.

By measuring the adsorption of NH_4-PMAA onto α-Al_2O_3 at different pH values, Cesarano, Aksay, and Bleier were able to develop a stability map for that system. The Al_2O_3 used had a surface area of 5.9 m^2/g, and the NH_4-PMAA used was Darvan C, with M_w of 15,000. This stability map is shown in figure 2. The curve represents a minimum adsorption level of PMAA needed to stabilize the suspension for different pH values. Below this level of adsorption, the Al_2O_3 powder is not well-dispersed due to bridging flocculation. The suspension is stable if the amount of adsorbed polymer is at or slightly above the curve.[21]

For most colloidal processes, a slurry with a very high solids loading level (>50 vol%) is desirable. The addition of polymer dispersant allows for well-dispersed high solids loading slurries to be created. Obviously, the loading is reduced by the amount of space taken up by the polymer. Thus, the theoretical maximum solids loading is impossible to attain in an electrosterically stabilized system. The amount of space occupied by polymer is dependent upon the length and morphology of the polymer chain

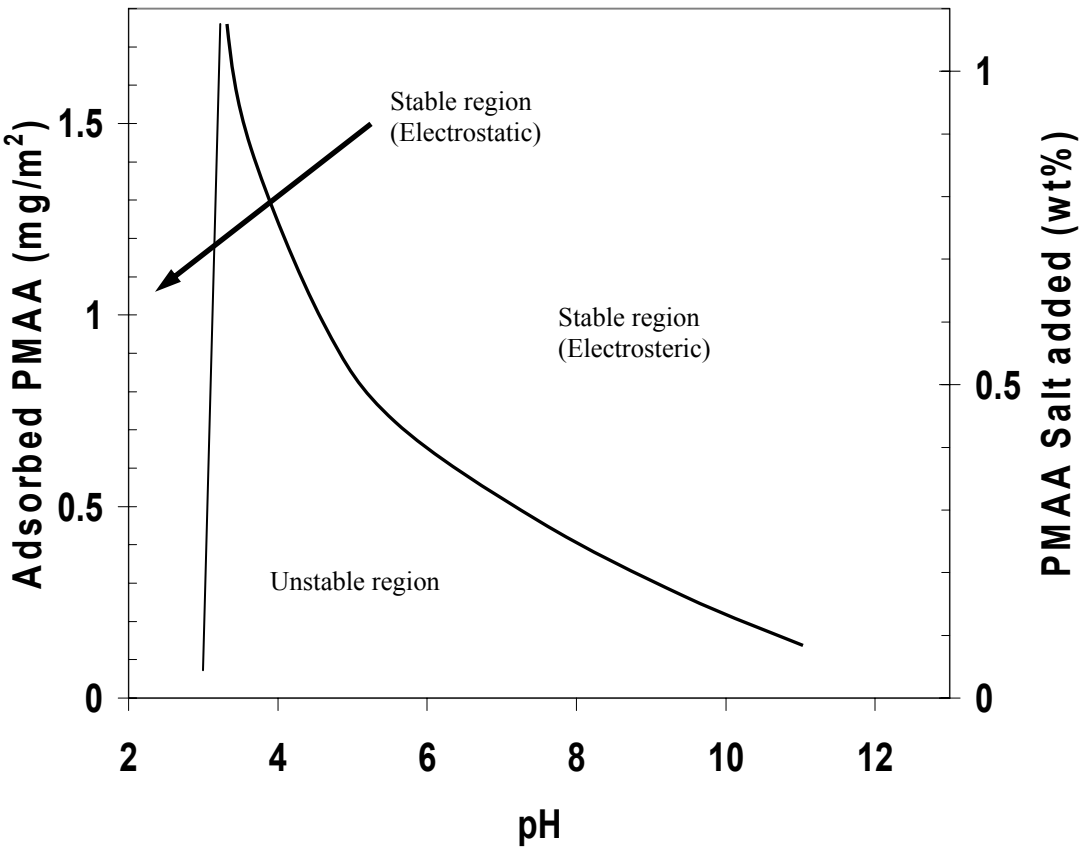

Figure 2. Stability map for adsorption of PMAA salt on α-Al_2O_3 with 5.9 m^2/g surface area (after ref. 22).

when adsorbed. Ideally, the adsorbed polymer layer should be just thick enough to prevent van der Waals bonding. Sigmund *et al.* calculated the effect of interparticle repulsion on relative packing density. Too short of a polymer chain will yield a small adsorption layer, resulting in flocculation due to van der Waals attraction, while excess length of the polymer chains will result in a dramatically decreased effective solids loading.22

To make densification simpler, we would like to prepare suspensions of ceramic particles with the highest solids loading theoretically possible. In practice, however, the solids loading achieved is often limited by the usability of the suspension; a nanoparticle suspension that does not flow well has little value. The ability of a liquid to flow can be quantified by its viscosity. A number of techniques exist to measure viscosity, but most commonly the fluid to be characterized is placed between two parallel plates that are moved relative to one another, and the shear stress and strain rate are measured. For a Newtonian fluid, such as water, viscosity can be considered a material parameter, which means viscosity can be mathematically defined as

$$\eta = \frac{\tau}{\dot{\gamma}} \qquad (1)$$

Where η is the viscosity, and τ and $\dot{\gamma}$ are shear stress and shear strain rate, respectively. However, most suspensions of ceramic particles are not Newtonian, and hence viscosity changes with strain rate:

$$\eta(\dot{\gamma}) = \frac{d\tau}{d\dot{\gamma}} \qquad (2)$$

Often, the viscosity of a colloidal suspension decreases under greater shear rate, resulting in shear-thinning behavior. [26,27,28]

As more solid particles are placed into the liquid system, it becomes more difficult for the particles to move relative to one another. The distance between particles has decreased, and more collisions between particles occur under shear. Krieger and Dougherty developed a mathematical relationship describing solids loading and viscosity:

$$\frac{\eta}{\eta_0} = \left(1 - \frac{\varphi}{\varphi_m}\right)^{-n\varphi_m} \qquad (3)$$

where η is the viscosity, η_0 represents viscosity of the suspending medium, and $\frac{\varphi}{\varphi_m}$ represents the particle packing over the total possible packing. Here, n is a function representing intrinsic viscosity. [29] A number of similar models have been expressed. As Liu showed, most of these equations describing particle packing-viscosity behavior follow the simple form of

$$\boldsymbol{1 - \eta_{r}^{1/n} = a\Phi + b,} \qquad (4)$$

where η_r is the relative viscosity, n is a constant of the system (dispersant, solvent, powder used) and Φ is the particle packing density. Assuming that the system follows the model, the viscosity of suspensions of several different solid loading levels can be used to extrapolate a theoretical maximum, at the point where viscosity is infinite. [30] This phenomenological approach to calculating maximum solids loading is relatively simple.

1.3.D What are colloidal dispersions used for?

One of the most common and industrially important techniques of forming is slip casting. The slip is prepared from ceramic powder, dispersed in water. A mold is made of gypsum (plaster), which can take complex shapes, although undercuts may be difficult. The mold must be porous, and can be reused, although its effectiveness may suffer. This technology is used on a wide scale to produce very large parts.

Although slip casting has been a widely used forming method for many years, the kinetics of drying the slip are actually quite complex. Capillary pressure in the mold sucks the water out, resulting in a condensed layer of particles at the mold wall, also called the "cast" layer. Additional water removal is then dependent upon water permeating through the cast and into the mold, or evaporating into the air. As the cast is formed, a pressure gradient is developed through the wall of the mold, and through the cast. This means that an optimum time will yield a certain cast thickness, after which additional consolidation will take more time. The pressure generated is dependent upon the pore size. As pores decrease in size, capillary pressure increases, however, permeability of water into the mold decreases. There is an optimum pore size for each system and desired thickness of the cast. Large solid parts can be made by slip casting, although the drying process can be quite long.

In tape casting, a suspension of powder is prepared in a liquid, usually an organic solvent or water. The slurry is placed into a hopper, and dropped onto a polymer tape or other substrate and smoothed out by a doctor blade. The solvent evaporates, leaving a flexible green tape. High amounts (as much as 10%) of binder and plasticizer are added in addition to the dispersant to impart the necessary flexibility. Tapes can be produced in the range of 10-1000 microns in thickness. The density of the cast, dried tape is low due to the high organic content, but high relative density can be achieved after sintering.

Tape casting has the advantage that it is possible to make very thin sheets of material, virtually impossible to accomplish by other methods. Thin sheets of ceramic material are useful for microelectronics, for example. Tape casting has a distinct disadvantage that it is only possible to make thin sheets. Laminated structures of many

cast tapes have been created, but structural parts are not practical through tape casting. Usually the solvent is a somewhat volatile organic compound such as trichloroethane, and many other complex organic compounds may be added as plasticizers or binders, which are undesirable because of toxicity, but aqueous suspensions have been used successfully. Tape casting defects include air bubbles, particle segregation (due to poor dispersion of powder with wide particle size distribution) and binder segregation. As binder moves to the surface of the tape, a density gradient in the ceramic is developed. During sintering, the density gradient can cause warping in the tape.

1.4 Freeze casting

1.4A Flow chart and description

Freeze casting is a novel ceramic forming process using colloidal techniques. A well-dispersed suspension of ceramic nanoparticles is poured into a mold, giving it shape, and is then frozen to impart strength during drying. The cast part is subjected to a vacuum, and the ice sublimates away, leaving a green compact. The freeze casting process is detailed in the figure 3 below.

1.4B Advantages of freeze casting

Compared with similar processes such as slip casting and tape casting, freeze casting offers several distinct advantages. Because freezing of water is used to impart strength during drying, the binder content is relatively low, while solids loading is still high. The dispersion medium, water, is non-toxic, and relatively inexpensive. Because the organic content is so low, typical problems associated with tape casting, such as particle segregation, and slip casting, such as complex drying procedures, are eliminated. The

mold materials for freeze casting are relatively inexpensive. Freeze casting can be performed in a flexible silicone mold, capable of holding fine details and intricate shapes.

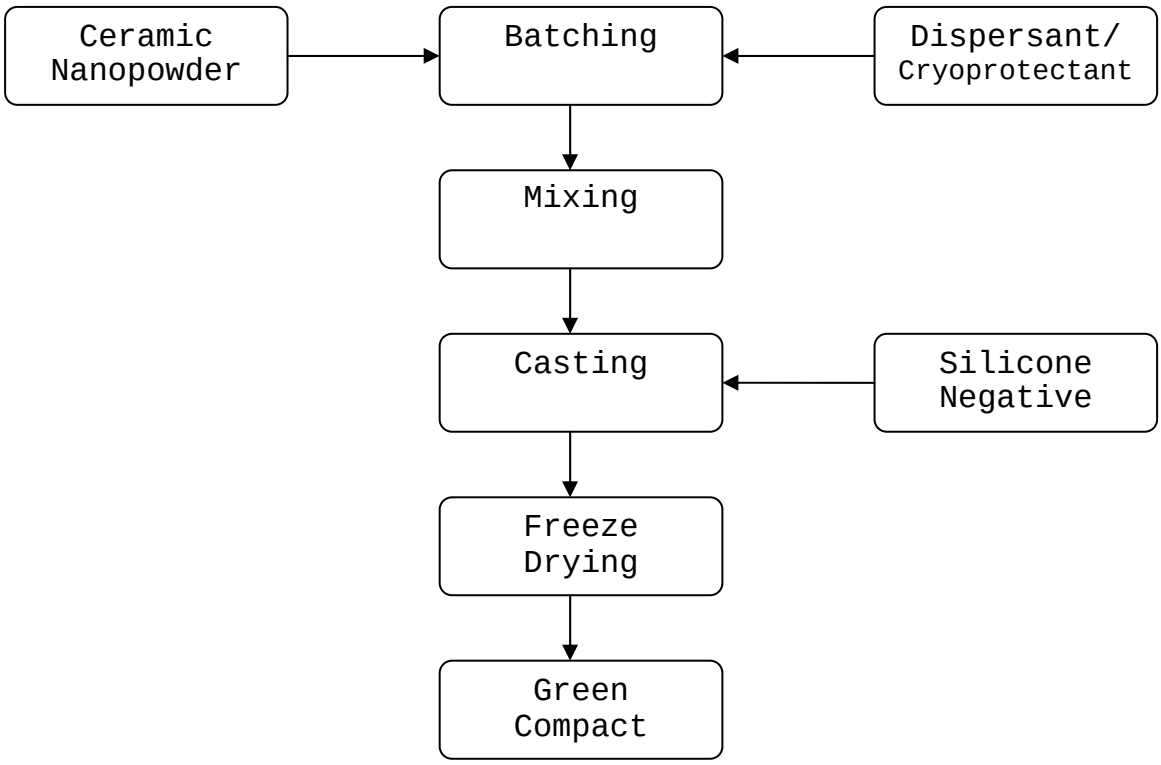

Figure 3. Flow chart showing the freeze casting process.

1.4C Problems with freeze casting

One of the most apparent problems with freeze casting is associated with the phase change of water. Water is one of few substances which expand upon freezing. The volumetric expansion can cause damage to a mold or container. Also, when water freezes, any solute or suspended particles are expelled from the pure crystal as it forms.[31] Any pure ice crystals formed in the system during freezing will become pores after drying. If the ice grains were nanocrystalline, and uniformly distributed, any porosity

resulting from ice formation should also be uniformly distributed, and would be much easier to remove.

Although the binder content is very low, certain other additives must be included due to the nature of the process. As mentioned, relatively high amounts of a cryoprotectant agent such as glycerol are present. In addition to necessary dispersant and binder, other ingredients may be added to make the suspension more manageable, such as surfactants to make it flow better. While these substances assist greatly in forming the green part, they will not contribute to the properties of the dense ceramic body, and must be removed, adding steps to the procedure. However, these organic contents are quite favorable when compared to those required for tape casting.

1.4D Results of freeze casting work from literature

A number of works have been published reporting successful freeze casting of colloidal Al_2O_3 or SiO_2 suspensions. In particular, great emphasis has been placed on control of the ice formation, which has been shown to directly affect homogeneity and porosity of the green structure. Freeze casting has been used as an alternative method for sol-gel formation. It was found that sols that were aggregated did not freeze well, and that the dried sols avoided cracking due to large porosity in the green structure.[32]

Cooling rate of the samples has a dramatic effect on the microstructure of ice crystals. Koch *et al.* found that the structure of ice formed in an amorphous or ultrafine layer on the surface of the Al_2O_3 sample, while individual ice crystals could be seen one mm into the structure. Because of heating by thermal conduction, there was necessarily a gradient of the cooling rate inside the sample, and pore size increased as cooling rate decreased. The cooling rate of the sample will be affected by the starting temperature of

the freeze dryer chamber, the freezing temperature, and, less quantitatively, by the relative amount of insulation provided by the mold and any handling equipment, such as trays. Statham *et al*. found that a rapid cooling rate (~1000°C/h) results in fine, equiaxed particles, and low porosity in the green body, while slow cooling rates (~20°C/h) cause dendritic formations.[33] The same phenomenon may be considered in terms of purity of the ice crystals. At high cooling rates, ice crystals are more pure, segregating water from the suspended particles, while at lower freezing rates, it is kinetically possible for less pure crystals to form, although the addition of a cryoprotectant may prevent segregation of water over different freezing rates.[34]

Sophie and Dogan have shown that glycerol can be used effectively as a cryoprotectant in a water-based freeze casting system. Use of glycerol in an Al_2O_3-PMAA system had a dramatic effect on surface smoothness, microstructure, and allowed much higher green density to be achieved. Suspensions of Al_2O_3 were cast into bodies and sintered to full density at 1650°C with addition of 20 wt% glycerol to water, but could not reach 90% with just water.[48,49] The effects of glycerol will be discussed further in Chapter 3.

1.5 Al_2O_3 and Carbon Nanotubes

1.5A Early work and results

Carbon nanotubes have been successfully incorporated into a number of ceramic composite systems. CNTs have been added to ceramic-metal systems and consolidated by hot pressing, although the strength resulting from these techniques was less than desired, probably due to low density of the sintered material.[35,36,37] Hot pressing techniques have also been shown to partially or completely destroy the structure of the CNTs. Better

results have been attained through spark plasma sintering techniques, which allow a much greater density to be achieved in a shorter time.[38]

1.5B Problems associated with processing

In order to obtain a meaningful benefit from the addition of CNTs to a freeze cast suspension, the included CNTs must be uniformly dispersed; the composite structure should be homogeneous. Another limitation is the strength of the bonding in the composite material. If the bond is not sufficient to hold the CNTs in the matrix, there is no reinforcement. CNTs usually exist as a bundles or ropes, shown in figure 4, due to extremely high surface forces, and are notoriously difficult to separate into individual tubes. In order to allow the CNTs to become connected in the matrix (percolated), they must be separated into individual tubes. CNTs, like graphite, will oxidize at the temperatures necessary to densify ceramics.

A number of approaches have been attempted to separate CNTs, including surface treatments,[39] functionalization,[40] and adsorption of different dispersants.[41] The most common method used for dispersing CNTs in liquid is through the addition of a dispersant, such as sodium dodecyl sulfate (SDS), followed by extensive ultrasonication.[42,43,44] Colloidal processing techniques have also been employed to coat the surface of CNTs in suspension with oxide particles. Such an approach has the advantages of ensuring that the CNTs are easy to disperse, and that there is strong interfacial bonding between the ceramic matrix and the CNT reinforcement. This approach has been used to prepare a composite Al_2O_3-CNT powder that was successfully hot pressed to >90% relative density.[45] In a similar approach, CNT-$BaTiO_3$ composite material was prepared by immobilizing TiO_2 onto the surface of CNTs and ball milling

the hybrid TiO_2-CNTs with $BaTiO_3$ powder. 0.1 wt% CNT composites were prepared to 99% theoretical density by this approach.[46]

1.5C What areas need to be explored?

In order to successfully incorporate CNTs into a ceramic composite, the interactions between the CNTs and the other components of the system must be carefully monitored. Dispersion of the CNTs is dependent upon coating them with a polymer, or

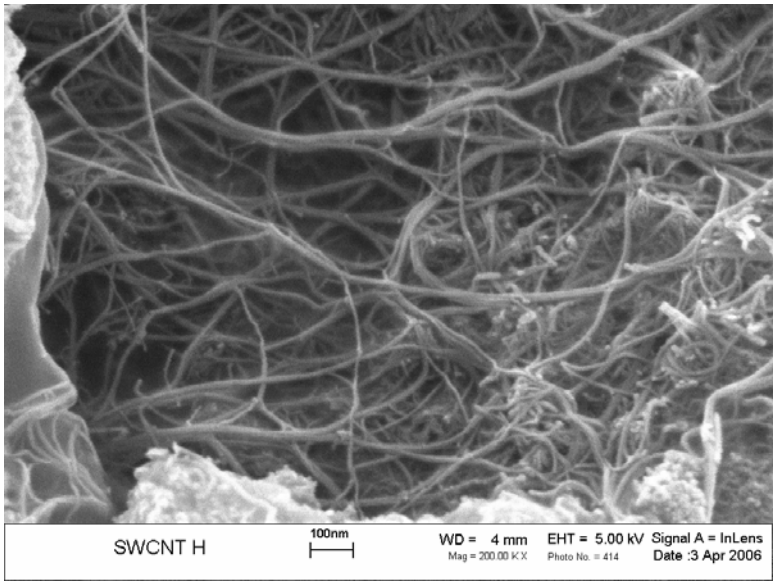

Figure 4. SEM image of carbon nanotubes.

with an oxide. By ensuring that the pH is maintained at the appropriate level, and that the correct dispersants are chosen, it should be possible to disperse the CNTs in water and prepare a compatible oxide dispersion. The sintering must be executed in such a way that the CNTs are not allowed to oxidize. It may be possible for this to be accomplished in an inert atmosphere or in vacuum.

Chapter 2. Research Plan

ABSTRACT

The goals for the project are to develop a procedure that can inexpensively create nanostructured ceramics with homogeneous microstructure via freeze casting. The dispersion state of the Al_2O_3 particles will be optimized, and MWCNT- Al_2O_3 composites will be created. The mechanical strength of the green parts will be determined. A densification procedure will be developed, and the densified parts will be characterized.

2.1 Motivation

The ultimate goal for this project is to develop a simple and inexpensive method of preparing nanostructured ceramics with homogeneous microstructure, with the ability to make complex shapes and surface details. The avenue of exploration chosen to pursue this goal is colloidal processing and freeze casting. The capability of this method in regards to production of MWCNT–Al_2O_3 composites will also be examined.

2.2 Dispersion

2.2A Electrosteric stabilization

First, the optimum conditions for dispersion of Al_2O_3 in water will be examined to allow the maximum solids loading with the best flow characteristics. Specifically, suspensions will be made to quantify the effects of different amounts of a polymer dispersant at fixed solids loading and pH, different pH at fixed dispersant amounts, and different solids loading with fixed pH and dispersant amount. These parameters will be combined to determine the best conditions to promote dispersion. The highest solids loading possible will then be determined.

2.2B CNT

A MWCNT- Al_2O_3 composite will be made via colloidal processing. Specific attention will be paid to the surface charges of the Al_2O_3 and CNTs in the suspension with the goal of preventing agglomeration of the CNTs. As high solids loading of CNTs as possible will be included to generate a network of CNTs that will affect the electrical properties of the system.

2.2C Characterization of dispersion

To characterize the quality of the dispersion, several techniques will be employed. A high zeta potential indicates good dispersion characteristics. Zeta potential of the suspensions will be measured using dynamic light scattering equipment. The adsorption of polymer onto the ceramic nanoparticles will be determined via potentiometric titrations. Viscosity of the suspension is of critical importance for our application. Also, storage modulus and loss modulus can give a good idea of the suspensions' behavior under shear, also important in our application.

2.3 Freeze casting

2.3A Development of freeze casting procedure

After the suspension has been optimized from a dispersion standpoint, a procedure for freeze casting must be developed to freeze cast the Al_2O_3 suspensions. Suitable molds will be created that will allow easy freezing and de-molding of the samples, while imparting a relatively complex shape to the green Al_2O_3. The procedure will be adjusted to yield a homogeneous and defect free microstructure, if possible.

2.3B Freeze casting profile

The freezing time, cooling rate and temperature are important factors to consider. The ultimate goal of controlling freezing is to obtain an advantageous microstructure in the ice formed, with a homogeneous distribution of nanocrystalline or amorphous ice only present. Poor microstructure of the ice will cause poor microstructure of the green compacts produced.

2.4 Characterization of green parts

2.4A Density and microstructure

Once parts have been freeze cast, the quality of the parts in the green state will be assessed by measuring physical properties. The density of the green part will give an idea of the quality of dispersion of the original suspension, as well as the suitability of the freeze casting procedure used. The microstructure will be examined using optical and electron microscopy. A defect-free, homogeneous structure is desired for ease in densification.

2.4B Flexural modulus/mechanical properties

The mechanical strength of the green material will also be characterized. The strength of the samples will give an idea of how easy it will be to handle the green compacts, as well as give some comparison to the quality of the green parts relative to other forming techniques. The green strength may also be used to compare the relative quality of suspensions with different amounts of MWCNT.

2.5 Sintering

2.5A Development of sintering procedure

The green compacts developed by the freeze casting process (like virtually any ceramic forming process) are not immediately useful. The parts must be densified to take advantage of the properties of the bulk ceramic material. Sintering procedure will be explored for suspensions with Al_2O_3 and those of Al_2O_3 and MWCNT. The green parts will be heated to remove the organic content, then to densify the powder.

2.5B SEM of sintered sample

The sintered Al_2O_3 parts will be characterized to determine their relative quality. The density will be examined to determine if suitable densification has been attained. The samples will be examined with a Scanning Electron Microscope to determine if the internal structure is uniform and free from porosity.

2.6 Uniqueness

The process of freeze casting provides several distinct advantages. Colloidal processing should yield a uniform microstructure, and comparable green density compared to dry pressing but lower tooling costs. Because it is flexible and inexpensive, the mold used can take any shape at a relatively low cost. There is also the potential to develop MWCNT-Al_2O_3 composite materials that are uniform in structure and composition, a goal that has challenged ceramists due to the unique aspect ratio and surface properties of MWCNT.

Chapter 3. Experimental Procedure

ABSTRACT

The materials used in the project, such as Al_2O_3 nanoparticles, polymer dispersants and MWCNT, are characterized. The polymer dispersant and Al_2O_3 were added to a glycerol-water premix, and ball milled to promote mixing. The levels tested for optimization of dispersant amount, pH and solids loading of the suspension are listed. Potentiometric titration and rheology testing, were used to determine dispersion quality, and the concentric ring test measured green strength. The procedure for making suspensions of MWCNT-Al_2O_3 is very similar to that for pure Al_2O_3. A freeze cast temperature of -35°C and time of two hours were chosen based on literature. The sample discs for the concentric ring test were prepared from aluminum discs of 1" x 1/16".

3.1 Suspension design

Suspensions were prepared with the materials shown in Table 1. Vendor information is included for each material used.

Table 1. Materials used in preparation of Al_2O_3 suspensions.

Material	Vendor	Location
Al_2O_3 powder	Nanophase Technologies	Romeoville, IL
Glycerol	Fisher Scientific	Fairlawn, NJ
PAA	Sigma Aldrich	St Louis, MO
Carbon nanotubes	Helix Material	Richardson, TX
NH_4-PMAA (aqueous)	R. T. Vanderbilt Co	Norwalk, CT
HCl, aqueous	EMD Chemical	Gibbstown, NJ
NH_4OH, aqueous	VWR International	West Chester, PA

3.1A Nanodur powder – characterization

Nanodur Al_2O_3 powder (Nanophase Technologies, Romeoville, IL) was chosen because of its commercial availability. It has a relatively small particle size (38 nm) which is desirable to make a bulk sintered nanocrystalline part. The vendor reports a phase distribution of 70:30 δ:γ Al_2O_3, with a theoretical density of 3.6 g/cm^3, and specific surface area of 45 m^2/g. Particle size was characterized with TEM and with a Malvern Nano ZS Zetasizer (Malvern Instruments, Southborough, MA). The TEM image and particle size distribution of the powder are shown in figures 5 and 6. The results are consistent with the vendor's data of 38 nm average particle size. The particle size

analysis shows a bimodal distribution, with the main peak centered near 30 nm, and a secondary peak at about 190 nm.

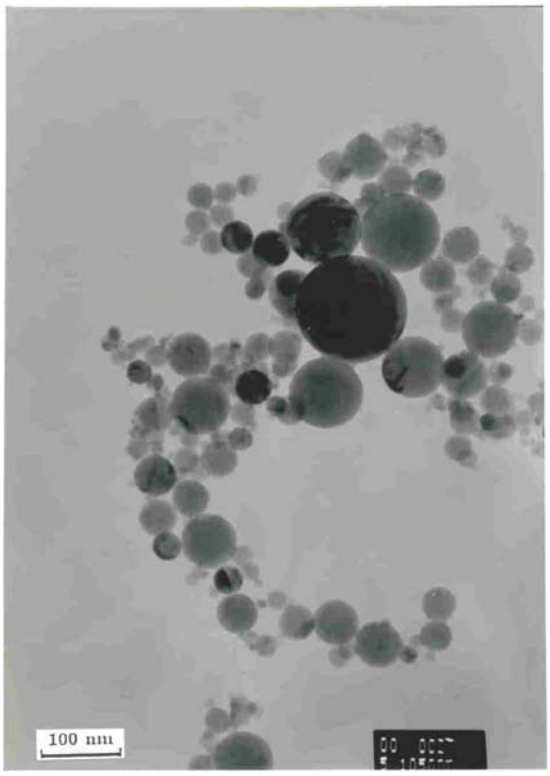

Figure 5. TEM image of Al_2O_3 powder

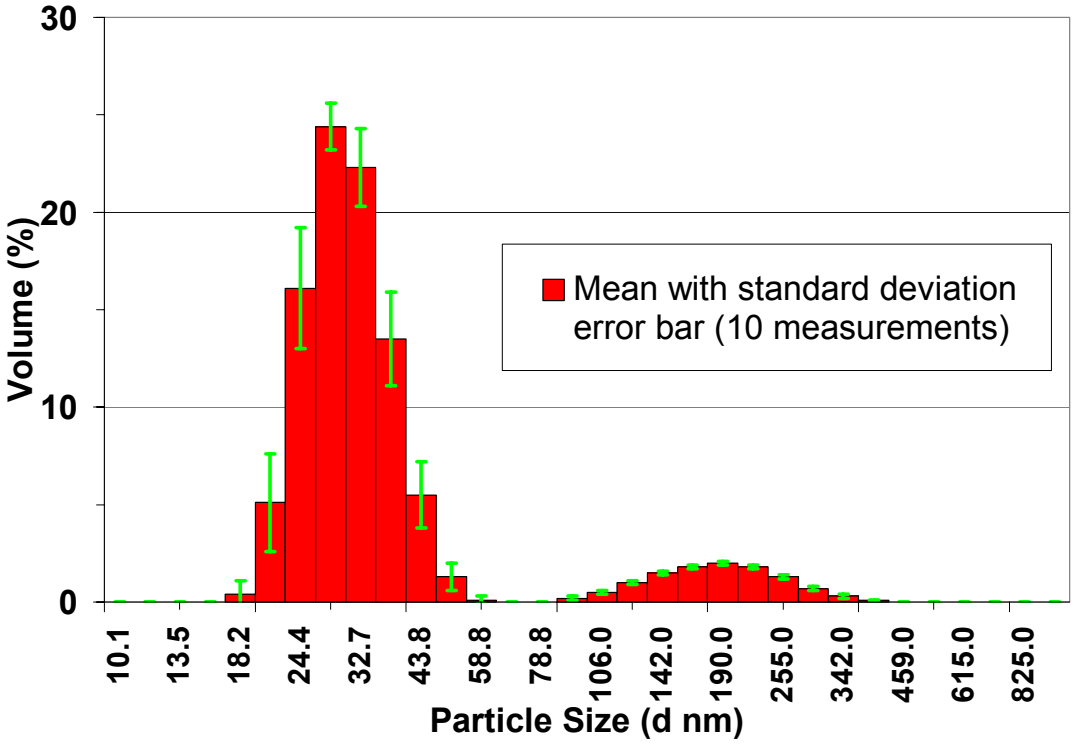

Figure 6. Particle size distribution of Nanodur Al_2O_3 powder (volume based). Measured with Malvern ZetaSizer Nano.

3.1B Glycerol

Previous attempts to prepare ceramic bodies by freeze casting have shown that the freezing of water causes large, dendritic crystals, resulting in similar pores in the green body, and that nanocrystals of ice or amorphous ice result in a more advantageous homogeneous microstructure.[47] The addition of a certain organic species has been shown to inhibit crystallization of ice, resulting in an amorphous structure. Any potential organic used as a freezing agent must be inexpensive, must be soluble in water, and must lower the melting point of water as little as possible. Sophie and Dogan have shown that additions of glycerol to the slurry allow the microstructure of ice to be controlled.[48,49] Glycerol is commercially available, having a simple alcohol structure shown in figure 7,

and exists as a viscous, clear liquid at room temperature. Because of its highly polar nature, it is totally miscible in water. Although the viscosity of water increases slightly from the addition of 10 wt% glycerol,[50] suspensions of 60 vol% solids loading have been shown to be less viscous when made with a mixture of water and glycerol than with just water. Glycerol bonds with the hydrogen atoms in water, disrupting normal crystallization of ice.[29,46,47,51] The freezing point depression of water with 10 wt % glycerol is -1.6°C. Glycerol also has the advantages of slightly lowering the volume expansion of water upon freezing, and improving the heat transfer rate of water, allowing freezing to occur more uniformly, and preventing dendritic ice structures.

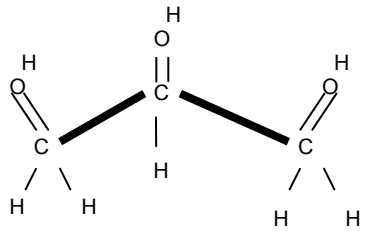

Figure 7. The chemical structure of glycerol.

3.1C Solids loading of suspensions

Initially, 20 vol% solids loading was used following the literature, particularly work done by Cesarano who conducted stability studies on both PMAA and PAA systems.[18,21] The slurry can be benchmarked and compared to similar work, before the solids level is increased. Lower solids loading level is also desired to ensure thorough mixing initially.

3.1D Dispersant

For the purposes of stabilization of the suspension in water, a polymer dispersant is needed. Based on the literature, different carboxylic acids were examined as potential dispersing aids, poly(acrylic acid) (PAA) and poly(methacrylic acid) (PMAA). PAA is commercially available at smaller size (Mw=1800) than PMAA (Darvan C, Mw=15,000). At higher solid loading, the volume of polymer added will become very important. Figure 8 presents the single unit structure of PAA.

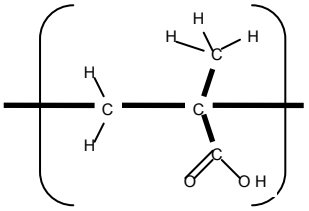

Figure 8. The single unit structure of poly(methacrylic acid).

A widely commercially available ammonium salt of PMAA (Darvan C, R.T. Vanderbilt Co, Norwalk, CT) was selected, based on literature. Darvan C is an aqueous, water-based liquid containing 30 wt% NH_4-PMAA (M_w=15,000), that is widely used in clays. PAA powder with molecular weight M_w=1800 (Sigma Aldrich, St Louis, MO) was obtained as well. The single unit structure of PMAA is shown below in figure 9.

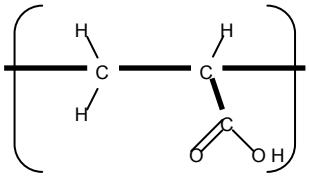

Figure 9. The single unit structure of poly(acrylic acid).

3.1E Processing and mixing

Ammonium hydroxide (NH_4OH) and hydrochloric acid (HCl) were chosen to adjust pH because of their high ionization and commercial availability. It is desirable to exclude sodium, which may stay in the slurry and become an impurity in the finished parts. To promote mixing, Al_2O_3 milling media were placed into the jar, and the jar placed on rollers.

3.1F Carbon nanotubes

Multiwall carbon nanotubes (MWCNT) with outside diameter of 10-30 nm and length of 0.5-40μm were purchased (Helix Material Solutions, Richardson, TX). These MWCNT have density of ~1.8 g/cm^3, >95% purity, with <2% amorphous carbon, according to the vendor. A TEM image of a typical MWCNT used in this research is shown in figure 10.

3.2 Procedure for suspension preparation

For the preparation of suspensions, 2g (10 wt% water basis) of glycerol was weighed into a polypropylene bottle. 20 mL of water was then added, and milling media placed into the jar. The mixture was then homogenized for a few minutes using the rolling mill. 20g of Al_2O_3 powder was added in 10g increments, along with the appropriate amount of dispersant. The bottle was hand shaken to promote mixing.

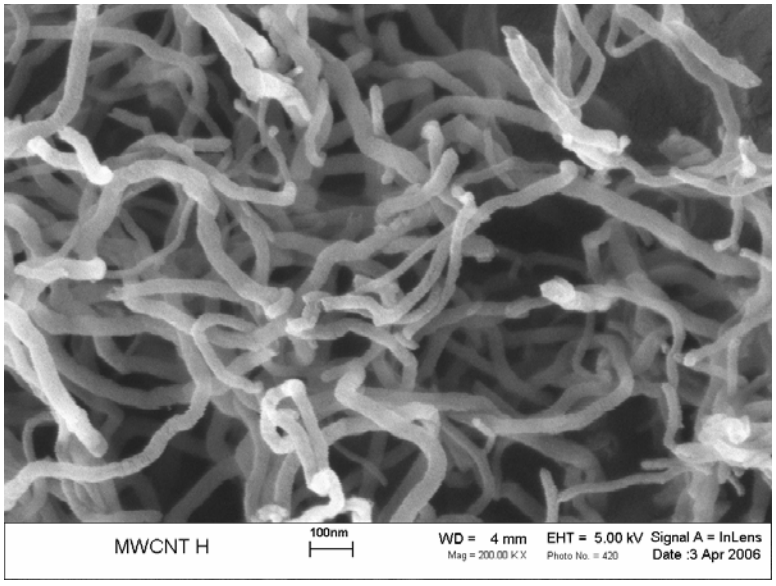

Figure 10. SEM image of multiwall carbon nanotubes used in this study.

This was necessary to reduce the apparent volume of the Al_2O_3, allowing more than 10g to be placed into the bottle at a time. It was noted that with the PAA dispersant, the mixture was very close to the zpc, so HCl was added to reduce the pH to around 1.5, to allow electrosteric stabilization and promote polymer adsorption. The slurry was then placed on the rolling mill and allowed to mix for 1 hour. After mixing, the pH of the slurry was checked, and adjusted if necessary. The slurry was then left to mix overnight. The pH was further adjusted by addition of acid, and allowed to mix for at least 30 minutes before rechecking the pH. The slurries were then allowed to mix for an additional two hours. This procedure was used to prepare suspensions of approximately 20 vol% Al_2O_3.

The pH was then adjusted to basic pH through the addition of NH_4OH. The pH was adjusted to 9.5 +/- 0.05. Al_2O_3 was added in 10 or 20 g increments, along with the appropriate amount of PAA. The bottles were shaken to promote mixing, and then placed onto the rolling mill for a time of one hour between additions. pH was measured and NH_4OH added as appropriate.

3.3 Zeta potential

Suspensions of Al_2O_3 were prepared with PAA and NH_4-PMAA dispersants using the procedure in section 3.2. Zeta potentials were measured using a Malvern 3000 Zetasizer (Malvern Instruments, Southborough, MA). Because of the limitations of the equipment, the suspensions had to be diluted to a 1:250 ratio for the purposes of measurement. The zeta potential of MWCNT were measured with a Malvern Nano ZS Zetasizer Nano (Malvern Instruments, Southborough, MA). 8 mg of MWCNT were added to 1 mM NaCl solution and the pH adjusted as appropriate. The addition of salt

was to ensure that the suspensions of MWCNT were of approximately uniform ionic content. The suspensions were then ultrasonicated for 2 hours.

3.4 Suspension characterization and optimization

3.4A Experimental design

For a suspension of ceramic particles to be effective for freeze casting, it must contain the maximum possible solids loading while still flowing well. To determine the optimum suspension, several variables were considered, including dispersant amount, pH value, and solids loading. Three sets of suspensions were prepared with different values for these parameters, and characterized based on flowability and adsorption of dispersant. The values for these parameters, shown in Table 2, were chosen based on work in the work by Cesarano *et al.* and preliminary results.

3.4B Adsorption – potentiometric titration

The method of potentiometric titration to determine amount of adsorbed polymer in a suspension has been used by Arnold and Overbeek in 1950, and later by Cesarano and Aksay, among others.[18,21,52,53] Potentiometric titrations were performed with NH_4-PMAA and PAA. Because the anionic polymer dispersants behave as weak polyprotic acids, there are two changes in slope of pH/titrant during the titration. The amount of titrant added between the two slope changes can be directly correlated to an amount of

Table 2. Levels used for optimization study.

Study of Dispersant Amount	Study of pH	Study of Solids Loading
pH=9.5 Solids loading = 30 vol%	PAA Amount = 2.00 wt% Solids loading = 30 vol%	pH=9.5 PAA Amount = 2.00 wt%
PAA Amounts (wt% of Al_2O_3)	**pH values**	**Solids Loadings (vol %)**
1.00	5.5	20
1.25	7.5	25
1.50	8.5	30
1.67	9.5	35
1.83	10.5	40
2.00		45
2.25		
2.50		

polymer in the liquid. Carefully measured amounts of carboxylic acid were added to water on a stir plate. The pH was adjusted to 9.5 +/- 0.05 pH before titrant was added, to promote dissociation of the acid in water, and pH was measured during the titration using a Denver Instruments model 250 pH meter (Denver Instruments, Arvada, Colorado). Adsorption calibration lines were developed for each polymer dispersant by titration of a known amount of dispersant. The calibration line should show a linear relationship between the amount of titrant used (number of ions) and the amount of polymer

dispersant being titrated. An example of a titration curve is shown in figure 11, and the calibration curves developed for PAA and NH_4-PMAA are shown in figure 12.

To measure the adsorption of each dispersant, appropriate suspensions were centrifuged at 2500 rpm for 45 minutes, and the resulting supernatant liquid was collected. A known volume of the supernatant was then titrated and compared with the adsorption calibration line to determine the amount of polymer remaining in the supernatant. From this value, the amount of polymer adsorbed for the entire suspension was calculated.

3.4C Rheology

One of the most important advantages of the freeze casting technique is the ability to generate complex shapes and sharp features. These features are dependent on the suspension flowing well into the mold. To quantify how well the suspensions flowed, a rheometer (AR 2000, TA Instruments, New Castle, DE) was used. The AR2000 rheometer is capable of measuring displacement and torsional and normal forces, which it uses to calculate the values of viscosity, storage and loss modulus, and adhesion characteristics, among many others. (For more information on calculation of these properties, see ref. 20.) It can use

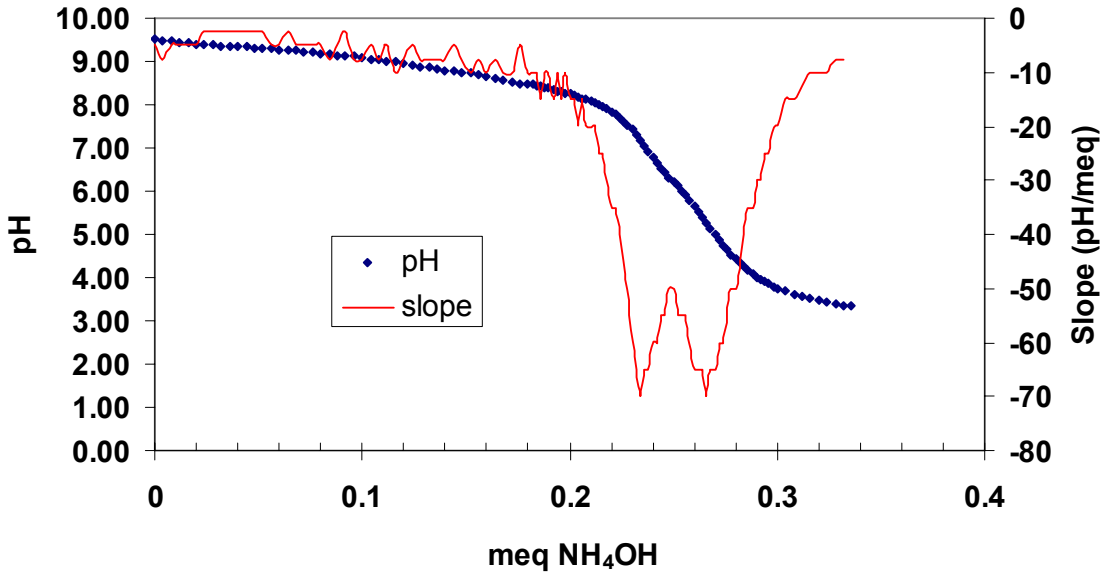

Figure 11. Example of data collected from a potentiometric titration. Starting pH was 9.5.

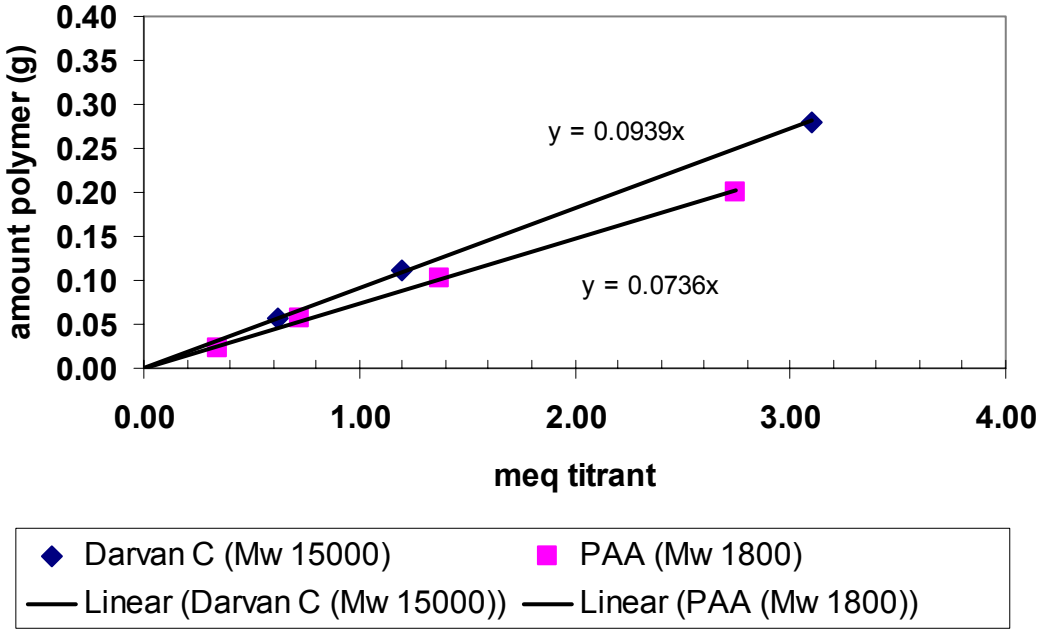

Figure 12. Calibration curve measured for titration of poly(acrylic acid), Mw = 1800 and poly(methacrylic acid), Mw=15,000.

either cone-plate or plate-plate geometries in shear stress controlled or shear strain controlled modes. The rheometer is pictured in figure 13.

The suspensions were examined in equilibrium shear rate controlled flow, at different levels from 10/s up to 200/s. A 40 mm steel cone with an angle of 2° and truncation gap of 54 μm was used for the cone-plate geometry. A solvent trap cover was used to prevent loss of moisture during the execution of all rheology testing. To ensure that all suspensions had a comparable shear history, an extensive pre-shear was performed up to a shear rate of 200/s. Each suspension was sampled and tested three times, and the average results plotted.

Figure 13. AR2000 Rheometer.

3.5 Preparation of suspensions with carbon nanotubes

To prepare nanoparticle suspensions of Al_2O_3 and MWCNT, the procedure is very similar to that in Section 3.2B. The MWCNT were added to the suspensions at a solids loading of 20 vol% Al_2O_3 immediately after change to pH of 9.5. MWCNT were weighed and added in increments of 100 mg. The suspension was allowed to homogenize for one hour. Al_2O_3 powder was added in 10 or 20 g increments, along with the appropriate amount of PAA, to yield suspensions of 40 vol% Al_2O_3 at pH 9.5. The bottles were shaken to promote mixing, and then placed onto the rolling mill for a time of one hour between additions. pH was measured and NH_4OH added as appropriate. All suspensions were ball milled for at least 24 hours prior to rheological testing. Table 3 shows the approximate amounts of MWCNT added to each suspension, and solids loading calculated from the actual mass of MWCNT added.

3.6 Freeze casting procedure

Suspensions of Al_2O_3 nanoparticles were freeze cast. First, a mold was made from a suitable object. The object was placed in a metal or plastic dish, and poly(dimethylsiloxane) epoxy (RTV 664, GE, Waterford, NY) was poured over the object and allowed to cure for 24 hours. The resulting mold was removed from the dish, and the object removed from the mold, exposing a cavity with the desired shape. A suspension of high solids loading (≥40 vol%) was poured in the silicone mold and allowed to flow so as to fill in corners and details. The filled mold was cooled from room temperature to -35°C in a freeze dryer (Labconco Stoppering Tray Dryer, Labconco, Kansas City, MO), shown in figure 14, and held for two hours to ensure thorough freezing

Table 3. Levels of MWCNT added to 40 vol% Al_2O_3 suspensions.

Suspensions prepared with Al_2O_3 and MWCNT pH=9.5 Solids loading = 40 vol% PAA Amount = 2.00 wt% of Al_2O_3	
MWCNT (g)	MWCNT solids loading
0.1	0.14 vol%
0.2	0.28 vol%
0.4	0.53 vol%
1	1.30 vol%
2	2.60 Vol%

Samples were removed from the molds, and the pressure was reduced to around 10 Pa and held for 36 hours at a temperature of -35°C, allowing frozen water to sublimate, leaving green compacts.

3.7 Mechanical testing of green specimens

3.7A Concentric ring test

The concentric ring test is a method of determining the strength of advanced ceramic materials.[54] It can be considered as a four-point bend test, if the fixture were rotated 360 degrees about the load axis. Hence, it has the advantage of isotropic test conditions, whereas the four-point bend test exerts high stress in the direction perpendicular to its supports.[55] The concentric ring design was conceived to eliminate

the effect of edge (corner) defects that result from the machining or shaping of a bar test specimen.[56]

Figure 14. Labconco Stoppering Tray Dryer

3.7B Test specimen preparation

Green Al_2O_3 discs were prepared for strength testing via freeze casting. Circular discs of 25.4 mm in diameter and 1.590 mm thickness were machined from aluminum. The aluminum discs were cast in poly(dimethylsiloxane) polymer (RTV 664, GE, Waterford, NY) to create suitable molds. A suspension of 40 vol% Al_2O_3 was prepared, and mixed via ball milling. The suspension was placed into the mold cavity using a disposable plastic pipette. Care was taken to completely fill the mold with the Al_2O_3 suspension to prevent large air bubbles. After mold filling, the samples were allowed to rest for one hour, and then frozen at a temperature of -35°C for 2 hours. The frozen discs were then removed from the molds and placed back into the freeze dryer. The freeze dryer chamber was evacuated to a pressure $< 10^3$ Pa, for 36 hours to sublimate the remaining ice.

3.7C Flexural modulus procedure and calculation

The equibiaxial flexural strength of green Al_2O_3 discs was determined, following ASTM C 1499. The samples were tested using a Texture Analyzer test console (Stable Micro Systems, Surrey, UK), equipped with a 5 kN load cell. A diagram of the Test fixtures and sample are shown in figure 15. Note the load ring and support ring (highlighted in black). A sample was aligned in the test fixture, ensuring that the load ring and support ring were concentric. To ensure uniaxial loading to the load fixture, a ball bearing was placed in the load fixture. The console was set to record compressive force, and the crosshead was lowered monotonically at a speed of 0.1 mm/min. The shape of the force vs. displacement curve was examined, and the peak force recorded. The fractured green sample was examined to ensure that the fracture mode conformed with a valid fracture per ASTM C 1499. The broken sample was measured with a digital micrometer to determine its exact thickness at the most likely crack initiation point. The equibiaxial flexural strength was then calculated for the sample, using the following equation:

$$\sigma_f = \frac{3F}{2\pi h^2}\left[(1-\nu)\frac{D_S^2 - D_L^2}{2D^2} + (1+\nu)\ln\frac{D_S}{D_L}\right], \qquad (5)$$

Where σ_f is the fracture strength in units of MPa, F is breaking load in units of N, h represents specimen thickness in mm, ν is Poisson's ratio for the material being tested, and D, D_S, and D_L are the sample diameter, diameter of the support ring and diameter of the load ring in mm, respectively.

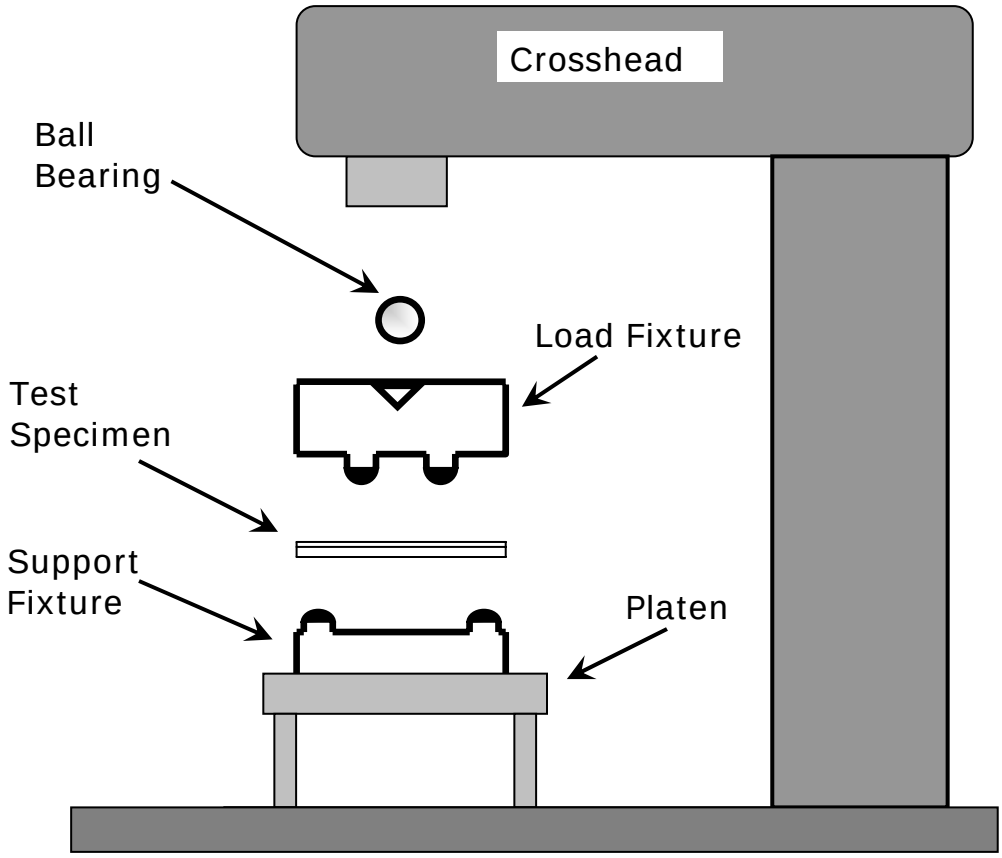

Figure 15. Cross-section view of the equibiaxial test apparatus, after ASTM C 1499.

3.8 Densification

3.8A Binder removal

In order to allow the organic species to escape from the sample, and to allow the powder compact to densify, it is desirable to remove the organic contents before sintering. Freeze cast Al_2O_3 samples were heated in air at a rate of <3°C/min, to a temperature of 450°C and held for two hours.

3.8B Densification

For purposes of densification studies, the samples were placed into a Netzsch 449A Dynamic Thermal Analyzer (Netzsch, Selb/Bavaria, Germany). The sample was heated

in air to 450°C and held for five hours, then heated at 45°C/min to a temperature of 1500° and cooled to 1265°C. The sample was held at 1265°C for ten hours to allow the sample to densify. The purpose of heating to 1500°C is to mobilize pores in the lattice, which promotes densification. Once the pores are mobile, the temperature is cooled to prevent grain coarsening.

Chapter 4. Results and Discussion

ABSTRACT

This section discusses experimental results and attempts to correlate those results with theory. The PAA dispersant was better than PMAA based on adsorption and dispersion data. Using PAA as a dispersant, the optimum values of pH, dispersant amount, and solids loading were characterized based on adsorption and rheology, and were determined to be 9.5, 2.00 wt% of Al_2O_3, and 40 vol%, respectively. Based on the viscosity data, the theoretical maximum for solids loading was calculated to be 50.7 vol%. An Al_2O_3 suspension with the optimum levels was successfully freeze cast, and the microstructure examined. Suspensions of 40 vol% and varying amounts of MWCNT were prepared and freeze cast. Strength of green samples was measured using the concentric ring test. Preliminary attempts at sintering were examined, and deemed to be unsuccessful at achieving full densification.

4.1 Zeta potential

Suspensions of 20 and 40 vol% were prepared with PAA and NH_4-PMAA at pH 9.5 and diluted. At pH 9.5, the polymer acid dispersants should fully dissociate, allowing direct comparison between PAA and NH_4-PMAA. The zeta potentials were strongly negative, <-40 mV for all conditions. Each of the conditions tested has a similar zeta potential. The zero point of charge for Al_2O_3 is slightly above pH 8, which indicates that the adsorbed polymer is the main contributor to the negative zeta potential. In general, a suspension is considered well dispersed if the absolute value of zeta potential is greater than 25 mV. The surface conditions of the suspensions were very similar.

The zeta potential of MWCNT at pH 3 was found to be 20.1 mV, and -30.4 mV at pH 9.5. These data are similar to results published by Sun and Gao, who report a zpc of MWCNT close to pH 6.[39]

The zeta potential must be considered when preparing the suspensions with MWCNT. Species with opposite surface charge will heterocoagulate. Based on the zeta potential values for Al_2O_3 and MWCNT, it was determined that the MWCNT should be added at high pH. At this condition, the MWCNT have a negative surface charge, and should not interact with the Al_2O_3 particles with adsorbed polymer

4.2 Examination of dispersants

For the purpose of freeze casting, a suspension that does not "flow" is not useful. In our experimental results, it has been shown that the maximum solids loading attainable is thus limited by viscosity. Preliminary results showed that slurry prepared with 2.20 wt% PAA with Mw 1,800 and pH 7.5 resisted flow at a solids loading of 36 vol%, while slurry prepared with 1.50 wt% PMAA with Mw 15,000 and pH 9.5 resisted flow at 16.9 vol%. NH_4-PMAA dispersant has M_w 15,000 and approximately 146 carboxylic acid groups per molecule. The PAA dispersant has M_w 1,800 and approximately 25 carboxylic acid groups per molecule.

Suspensions of 20 vol% Al_2O_3 were prepared, and the amount of the dispersants was carefully measured so that the carboxylic acid groups per mole of Al_2O_3 are the same

Table 4. Zeta potential of Al_2O_3 suspensions.

Solids Loading	Dispersant	Zeta Potential (mV)
20 vol%	PAA	-42.26
	NH_4-PMAA	-40.93
40 vol%	PAA	-41.10
	NH_4-PMAA	-43.35

at 0.028 mol. This equals to 2.78 wt% of Al_2O_3 for the NH_4-PMAA dispersant and 2.20 wt% of Al_2O_3 for the PAA dispersant. The difference in the dispersion efficiency should mainly come from the polymer-particle interaction, which is a function of polymer chain length and polymer molecular structure. For the NH_4-PMAA dispersant, the polymer chain is longer and there is a methyl group for each polymer segment. According to van der Schee's theory, the length of polymer molecule should not affect adsorption for a charged polyelectrolyte, for low ionic strength.[25] The methyl group may act as a shield, somewhat preventing adsorption of the polymer onto the oxide surface. For the lower molecular weight and shorter chain PAA, it is expected that more carboxylic acid groups will adsorb onto the nano-Al_2O_3 particle surface while the polymer chains extend into the suspension, which should provide strong dispersion. Potentiometric titrations of these suspensions were performed, and determined that 72.84 wt% of the NH_4-PMAA added adsorbed onto nano-Al_2O_3 particles while 75.73 wt% of the PAA added to the suspension was adsorbed.

Suspensions of different solids loading of Al_2O_3 nanoparticles were prepared with PAA and NH_4-PMAA as dispersants, and the viscosity measured. The results are shown

in figure 16. At low (20%) solids loading, both suspensions have relatively low viscosity, though the suspension prepared with PAA has slightly lower viscosity. As the solids loading is increased, the viscosity of the NH_4-PMAA- Al_2O_3 suspension increases much more sharply than that of the PAA- Al_2O_3 suspension, indicating that the PAA Al_2O_3 suspension is better dispersed.

According to the stability map generated by Cesarano *et al.* for PMAA adsorption in Al_2O_3 slurry, to stabilize a 20 vol% slurry at pH=9, approximately 0.35 mg/m^2 of polymer needs to be added (see figure 2). Correlating this to Nanodur Al_2O_3 powder (surface area = 45 m^2 /g), the minimum adsorbed amount for stability is 15.7 mg/g, or 1.57 wt% adsorbed. Cesarano and Aksay also found that the viscosity of slurries in

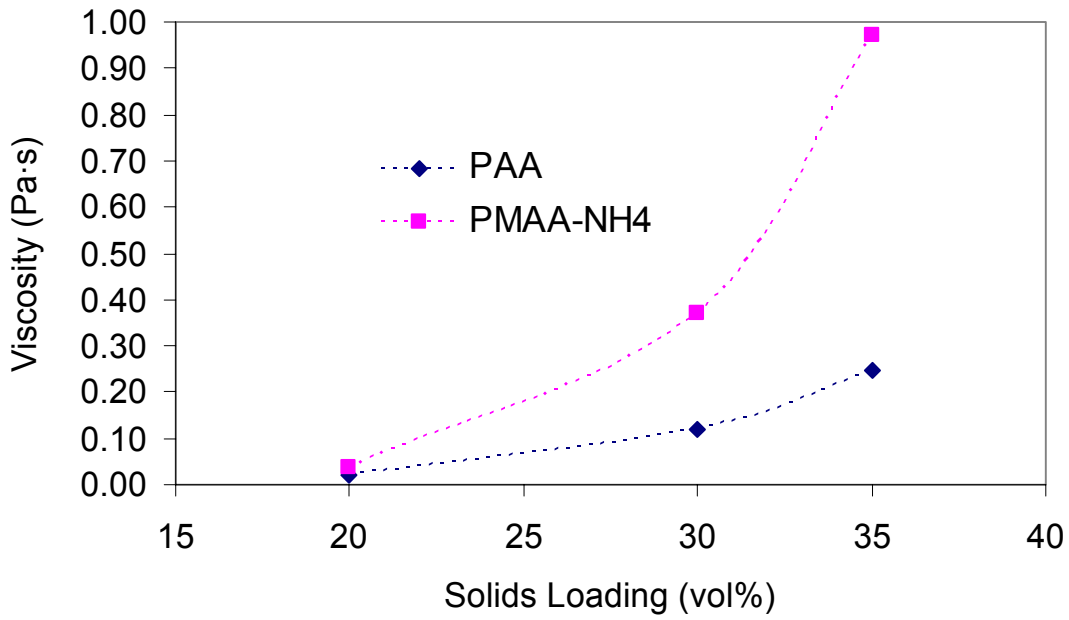

Figure 16. Rheological data for suspensions made with PAA and NH4-PMAA.

general decreased with the addition of more polymer, so more than 1.57% may be required. However, this model should serve only as a ballpark figure due to the high specific surface area of the NanoDur Al_2O_3 powder. With a solids loading value of 60%, for a 100 mL sample of slurry, there would need to be over 3 grams of polymer dispersant adsorbed to the powder in suspension. Later work also showed that with a lower molecular weight polymer, the viscosity is not as dependent on the amount of polymer added to the slurry. This may be because bridging flocculation is less likely to occur with a shorter polymer chain. In general, shorter chain length yields better performance. Based on these data, and the poor performance of the higher chain length polymer in preliminary work, the shorter chain length PAA is a better dispersant.

4.3 Adsorption results

4.3A. PAA amount and pH

Suspensions of 30 vol% Al_2O_3 were prepared with pH 9.5 and varying dispersant amount from 1.50 to 2.50 wt% (of Al_2O_3) The adsorption data calculated from potentiometric titrations are shown for these suspensions in figure 17. The adsorption of polymer was shown to approach a maximum value of 0.32 mg/m^2, at the level of 2.00 wt% PAA. At this level, a saturation adsorption level is attained and additional dispersant will not be adsorbed. Addition of additional dispersant may begin to cause depletion flocculation and increase viscosity. Examining the titration data, there is a linear correlation between the raw amount of polymer added to the suspension, and the raw amount of polymer in the clear supernatant.

Suspensions of 30 vol% Al_2O_3 were prepared with 2.00 wt% PAA and varying pH value from 5.5 to 10.5. The potentiometric titration data in figure 18 show that the

amount of polymer adsorbed decreases with increasing pH, which is in agreement with the literature. There appears to be a significant change in the adsorption kinetics around pH 8.5 which inhibits polymer adsorption. Purely by coincidence, this value is near to the published values for the zero point of charge of Al_2O_3 in water. It should be noted that due to the procedure for preparing the suspension, much of the adsorption of polymer species takes place at low pH.

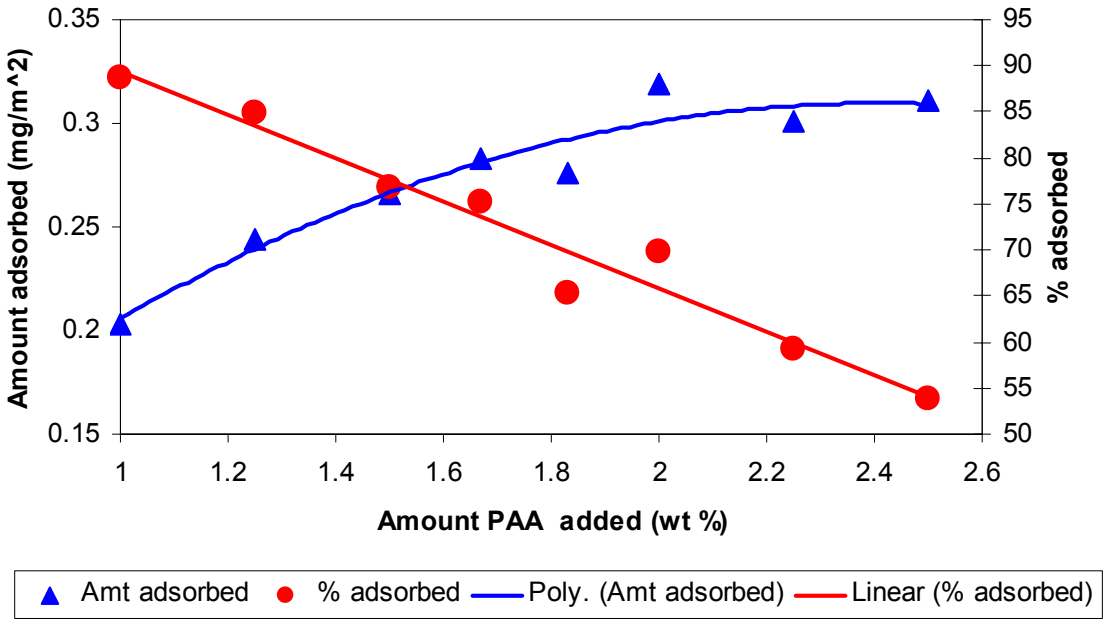

Figure 17. Polymer adsorption data for varying dispersant amount.

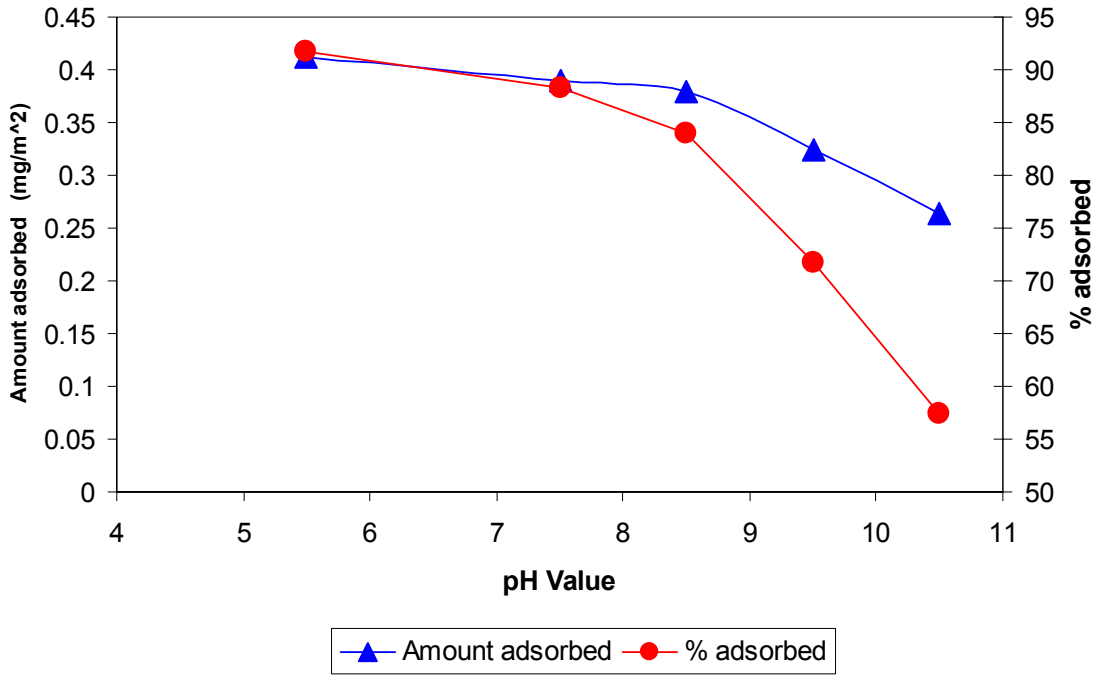

Figure 18. Polymer adsorption data for varying pH. All suspensions tested had 30 vol% Al_2O_3, and 2 wt% (of Al_2O_3) PAA.

The adsorption of the polyelectrolyte is clearly dependent upon pH, as well as the amount of free polymer in the liquid and the solids loading of the suspension. As pH increases, the anionic polymer acid dissociates, and net surface charge increases, however, the conformation of the polymer chain also changes, leading to a very different adsorption pattern: at low pH, the polymer dispersant adsorbs in a thin, high density layer, and at high pH, polymer adsorbs in a thick, low density layer.[20] In this case, the suspensions were prepared in such a way that some of the polymer was allowed to adsorb to the oxide at low pH, before the pH was adjusted to basic range. Because the powders were added to the suspension incrementally, the addition of PAA dispersant to the suspension, decreased pH significantly, and may have affected adsorption of the polymer

also. If the suspensions could be prepared in a continuous process, where powders were added in very small amounts so that pH could be kept at a constant value, the data might be more theoretically consistent. However, this method is neither practical nor economical for preparing any useful amount of nanoparticle suspension.

4.3B Solids loading

Suspensions with 2.00 wt% PAA and pH 9.5 were prepared, while varying solids loading from 20 vol% to 45 vol%. Adsorption data are shown for these suspensions in figure 19. Adsorption of the polymer increases from 0.31 mg/m^2 at 20 vol% solids loading to 0.36 mg/m^2 at solids loading of 45 vol%. The higher adsorption in higher solids loading suspensions is probably due to the interparticle distance. As the distance between particles becomes shorter, the likelihood of the polymer molecule overcoming the adsorption shielding effect improves.[21] The adsorption plateau will also be somewhat different for different solids loading levels, as compared with that for 30 vol% seen in Section 4.2A.

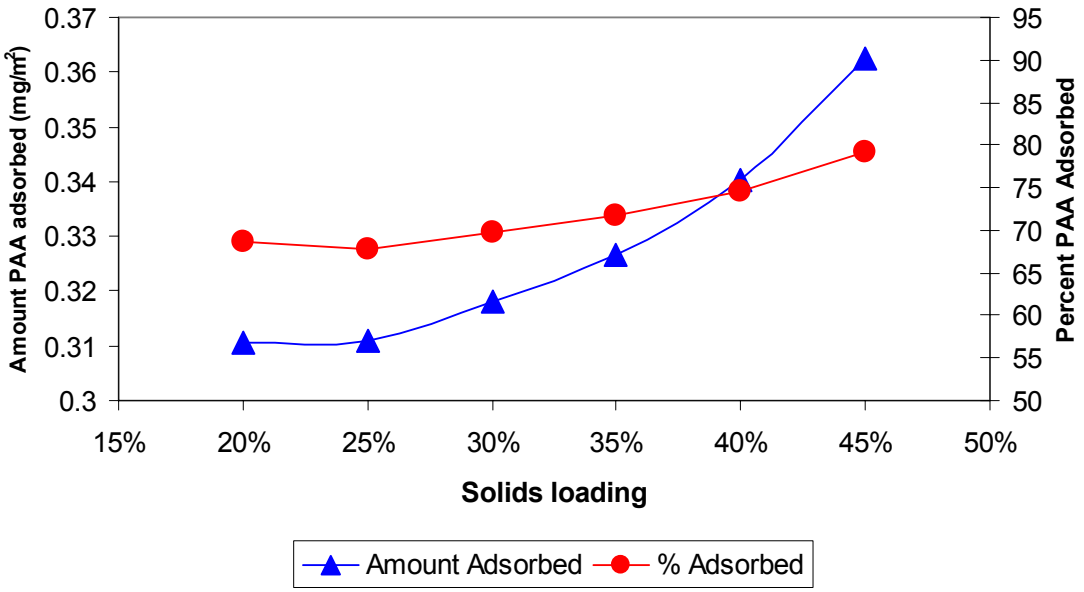

Figure 19. Polymer adsorption data for varying solids loading.

4.3C Adsorbed layer thickness

If the PAA were adsorbed in the high pH, low-density, fully-extended (100% "tail") configuration as shown in Fig. 1, the thickness of the polymer layer surrounding the oxide particles would correspond closely to the length of the polymer molecule. If the polymer were adsorbed onto the oxide nanoparticles exclusively in the high-density (train) configuration, the thickness of the adsorbed polymer layer could be estimated as the thickness of the repeat unit. The thickness of the adsorbed polymer layer could be estimated using the molecular weight of the polymer, and the carbon-carbon bond length. The vendor reports that the PAA used in this study has M_w=1800, and the repeat unit structure has a mass of approximately 72 AMU (see fig 13), and literature values for the C-C, C-H, C=O, and C-O bond lengths are 1.52, 1.10, 1.21, and 1.31A, respectively.[57] Maximum adsorption layer thickness for the high-adsorption mode should be ~0.5 nm

based on this approach, corresponding to a Γ value of 0.28 mg/m^2, which is less than the measured value 0.31 mg/m^2 for a 30 vol% Al_2O_3 suspension. These numbers are unrealistic based on the assumption of a linear polymer molecule adsorbed to the oxide surface. Based on the random coil configuration of a polymer, the molecular size, R_H, can be determined by the equation

$$R_H = 0.06(M_w)^{0.5} \qquad (6)$$

which yields R_H value of ~2.5 nm. Using the Krieger-Dougherty equation:

$$\phi_{eff} = \phi\left(1+\frac{\delta}{a}\right)^3, \qquad (7)$$

where ϕ_{eff} is the effective solids loading, ϕ is the solids loading of the Al_2O_3 nanoparticles, δ is the thickness of the adsorbed layer (or diffuse double layer, if it is thicker) and a the size of Al_2O_3 particles, the effect of the adsorbed polymer on solids loading can be estimated. For δ value of 2.5 nm, the effective solids loading ϕ_{eff} of a 40 vol% Al_2O_3 suspension is calculated to be 48.4 vol%. Guldberg-Pedersen and Bergstrom found that for polymer layers adsorbed at low pH, upon increasing the pH, the adsorbed layer thickness does not increase to a thickness corresponding to layer thickness of polyelectrolyte adsorbed at high pH. This may be due to the high density of the adsorbed layer, which hinders the expansion of the polymer upon conformational change.[58] However, based upon theoretical calculations of the electrical double layer thickness of the system performed elsewhere, it is clear that the adsorbed polymer layer (>2 nm) is much thicker than the diffuse double layer (<0.37 nm), and the effective solids loading is thus dependent on the adsorbed polymer layer.[59]

4.4 Viscosity results

By carefully examining the behavior of the aqueous suspensions under shear, we can better understand the nature of the system. Several rheological tests were performed, including steady-state flow to measure viscosity and oscillatory tests to measure viscoelastic properties.

4.4A Varying PAA amount and pH

Figure 20 shows flow behavior of suspensions prepared with varying amounts of PAA dispersant added. Suspensions were shear thinning for each amount of polymer tested. The suspensions show minimum viscosity for 1.83-2.25 wt% PAA. There was an increase in viscosity as the PAA amount increased from 2.25 to 2.50 wt%, which is most likely a result of depletion flocculation. Based on these tests, a polymer amount between 2.00-2.25 wt% is optimal.

Suspensions were shear thinning at each pH range tested. As figure 21 shows, the pH 5.5 suspension was by far the most viscous. For all shear rates tested, suspensions showed a decrease in viscosity as pH rose to 9.5, but an increase in viscosity from pH 9.5 to pH 10.5. This is most likely due to the decrease in the adsorption of PAA at pH higher than 8.5, which may have inhibited the steric component of stabilization.

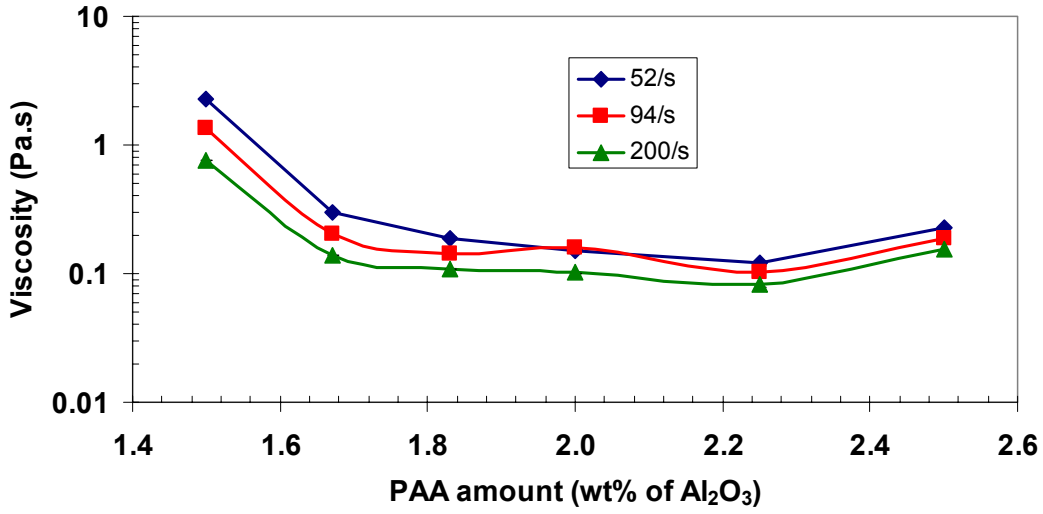

Figure 20. Rheology data for varying amounts of dispersant.

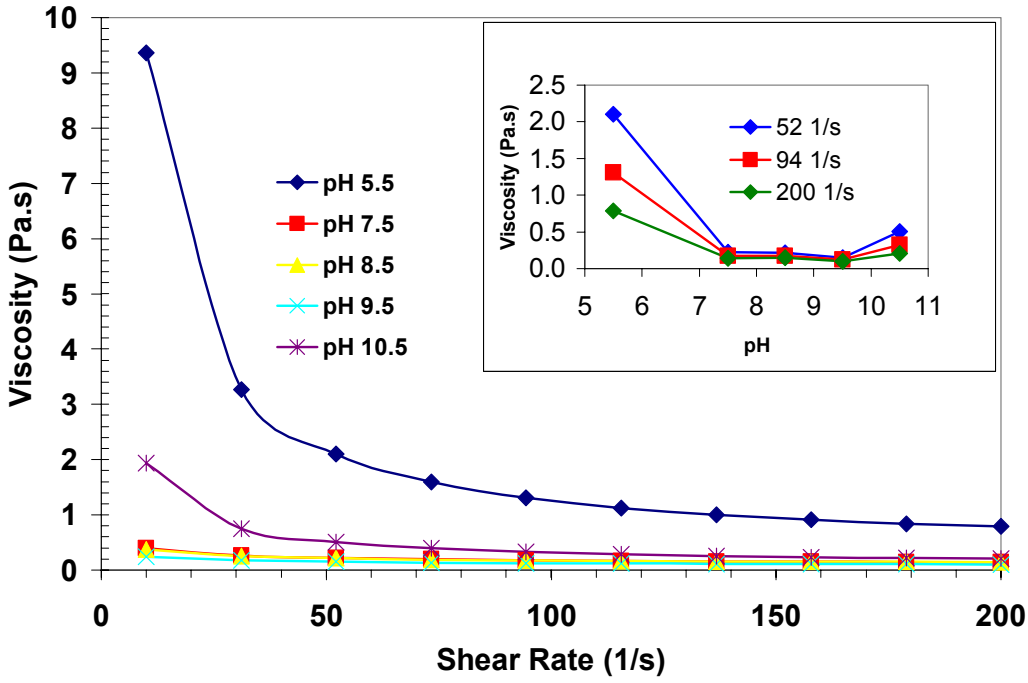

Figure 21. Viscosity for varying pH value. Inset: Curve showing viscosity vs. pH for three selected shear rates.

Although more polymer is adsorbed at pH 5.5 (41 mg/m^2 vs. 32 mg/m^2 for pH 9.5), the viscosity at pH 5.5 is much greater than at pH 9.5 for all shear rates, as shown in figure 21. This is due to configurational change of the polymer at high pH. The adsorption of the polymer onto the surface takes the train configuration at lower pH, while at higher pH, the polymer takes more of a loop or tail configuration, and less is adsorbed. Because both the ion cloud and the adsorbed polymer layer are much smaller, electrostatic stabilization is not effective at pH 5.5. Clearly, higher pH value (the tail configuration of polymer) is best for stabilization of a suspension, despite the fact that less polymer is adsorbed. A pH value of 9.5 provides the optimum viscosity for the suspensions tested.

4.3B Varying solids loading and maximum solids loading prediction

Figures 22 and 23 show viscosity and shear rate data for suspensions with different solids loading values. There is a two orders of magnitude difference in the viscosities of the 20 vol% and 40 vol% solids loading suspensions. Clearly, the internal behavior is quite different in these two suspensions when shear stress is exerted. All suspensions were shown to be shear thinning. For all solids loading levels, viscosity decreases logarithmically with increasing shear rate, as shown in figure 22. Figure 23 demonstrates that the sensitivity of viscosity to increasing solids loading increases with solids loading.

Based upon Liu's phenomenological solids-loading equation (equation 4), the maximum solids loading for this PAA-Al_2O_3 system was calculated. By plotting the solids loading, Φ, on the x-axis, and results of $1 - \eta_r^{-1/n}$ on the y-axis, the resulting plot yields a straight line. This line can be extrapolated to determine the amount of solids

which will cause the suspension to behave as a solid, which has infinite viscosity, at a value of $1 - \eta_r^{-1/n} = 1$. Although it is impractical to make a suspension with near-infinite viscosity, characterizing the system's maximum solids loading should give a good idea of the quality of our dispersion, and whether the solids loading used was appropriate.

Data showing the relative viscosity of Al_2O_3 suspensions with regard to solids loading ($1 - \eta_r^{-1/n}$ and Φ) are shown below in figure 24. Extrapolating the data to a value of infinite viscosity, it was predicted that the maximum possible solids loading for this system is 50.7 vol% Al_2O_3. It should be noted that this model assumes that first, an n-value of 2 is sufficient to characterize the 38 nm Al_2O_3 –1500 M_w PAA system at a shear rate of 94.45/s. Secondly, it is assumed that the model is valid over the entire solids loading range tested (20-45 vol%).[30] Although a solids loading of 50.7 vol% was never attained, a suspension with solids loading of 45 vol% was created and characterized successfully. From 40 to 45 vol%, viscosity increased from 0.91 to 2.24 Pa.s at a shear rate of 94.45/s. We can assume that an increase to 50 vol% Al_2O_3 would cause at least a similar multiple increase in viscosity, making the suspension totally unmanageable. It also should be noted that these solids loading levels do not consider the added thickness due to polymer adsorption. Applying equation (7) and assuming an adsorbed layer thickness of 2.5 nm, the effective maximum theoretical solids loading is 61.4 vol%, a number which compares favorably with theoretical values for random loose packing of monosized spheres.

Solids loading should be maximized to ensure good green density and assist in densification. However, the most important advantages of the freeze cast process include the ability to make intricate shapes and surface features, which requires relatively low

viscosity. A solids loading value of 40 vol% is less than half as resistant to flow compared to a suspension with 45 vol%. To ensure ease of handling and excellent mold-filling from the suspension, a solids loading of 40 vol% was used for freeze casting work.

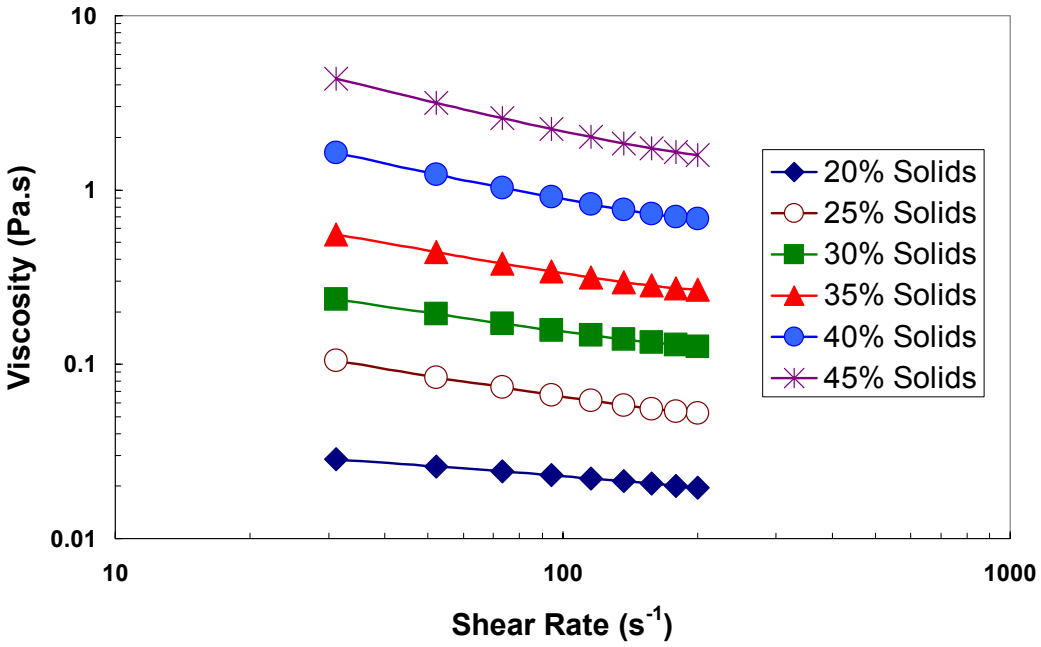

Figure 22. Rheology data for varying solids loading. All suspensions tested had 2 wt% PAA, and pH of 9.5.

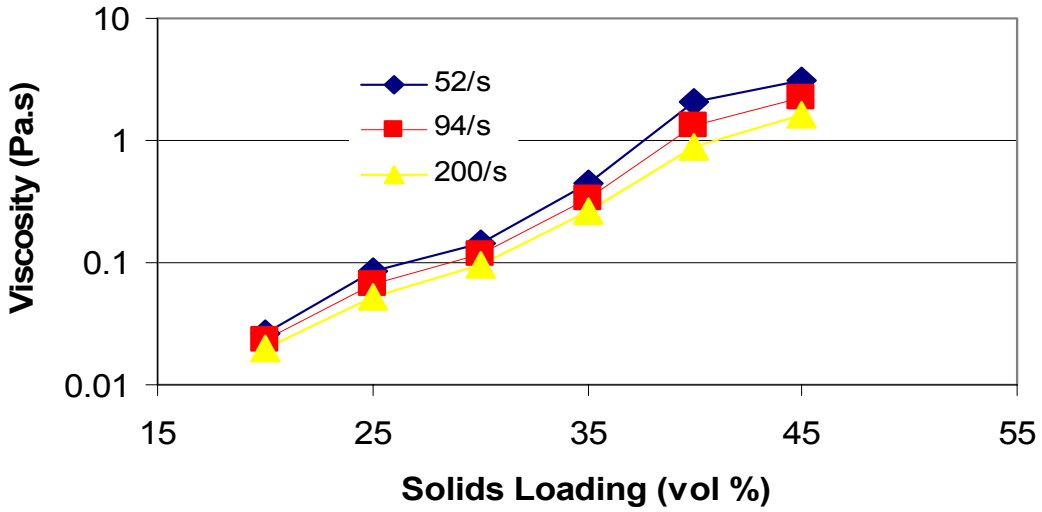

Figure 23. Al_2O_3 Solids loading effect on suspension viscosity.

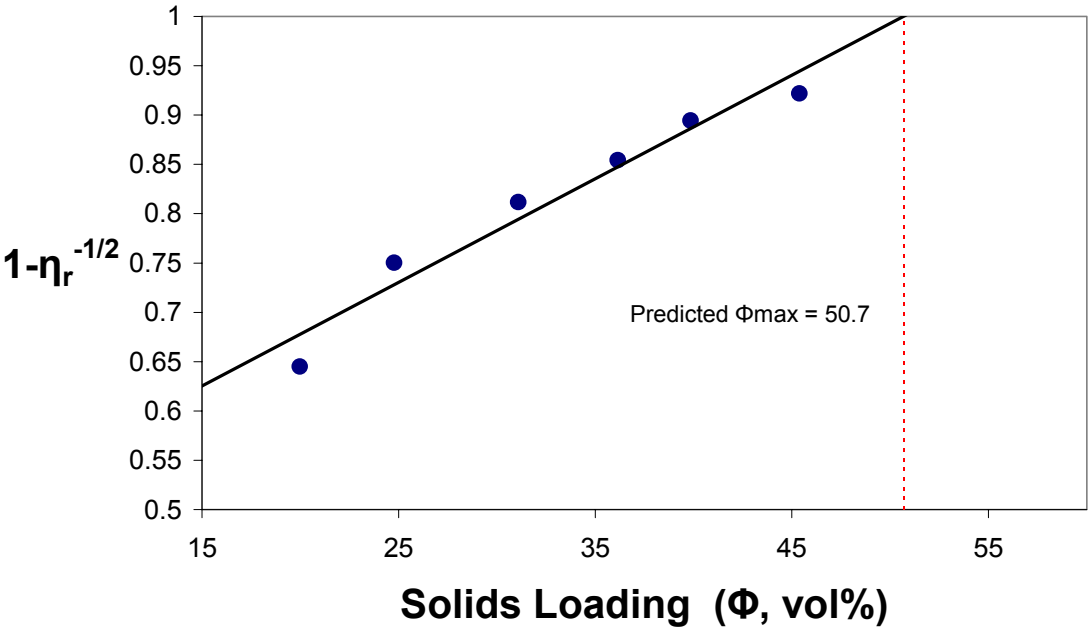

Figure 24. Prediction of maximum theoretical solids loading based on empirical data.

4.3C Rheology models and yield stress

As shown in Fig. 22, the suspensions exhibit differentially nonlinear behavior with shear rate increase. Even though many suspensions have been described by Newtonian flow at low solids loading conditions and by pseudoplastic flow at high solids loading conditions, it is desirable to analyze the Al_2O_3 suspension behavior by more exact flow models. To characterize the flow characteristics of the Al_2O_3 nanoparticle suspensions, different flow models have been examined, including Herschel-Bulkley model, Carreau model, Casson model, power law model, and Sisko model. Among all the models examined, the Herschel-Bulkley model describes the suspension behavior the best:

$$\tau = a + b\dot{\gamma}^{c} \qquad (8)$$

τ is the shear stress that the suspension experiences under shear rate $\dot{\gamma}$, ***a*** is the yield stress, and ***b*** and ***c*** are system-dependent constants. Figure 25 shows the excellent fit of the Herschel-Bulkley model for the Al_2O_3 nanoparticle suspensions at different solids loadings. As equation (8) shows, the Herschel-Buckley model represents both Newtonian flow and Bingham flow behaviors, when ***a*** is zero and ***c*** is unity for the first case and when ***c*** is unity for the second case. For the Al_2O_3 nanoparticle suspension, ***c*** is 0.71-0.77, meaning slower shear stress increase vs. shear rate than the Newtonian flow. Also, at high solids loading the Al_2O_3 nanoparticle suspensions exhibit non-zero yield stress ***a***, meaning the suspension has certain pseudoplastic flow behavior. Yield stresses are plotted by solids loading in figure 26.

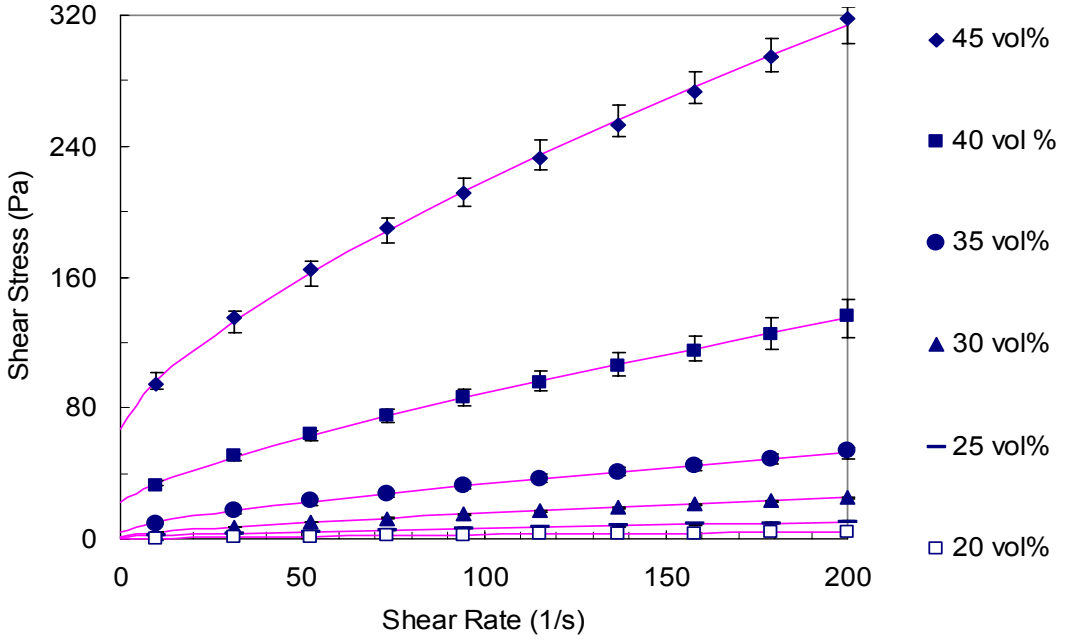

Figure 25. The rheology data are fitted to the Herchel-Bulkley flow model.

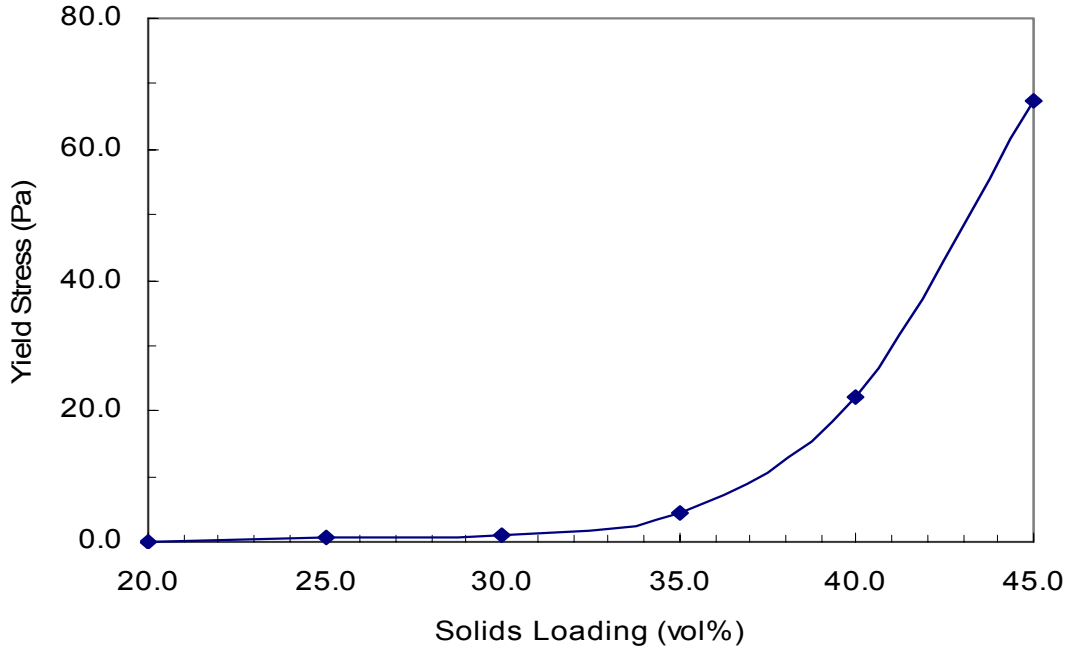

Figure 26. The yield stresses of different solids loading suspensions.

The yield stress can be considered a breakdown stress. Contact between the particles in the system is broken, and the suspension begins to flow under shear. Based on results from section 4.2, we can determine that the breakdown is an untangling of adsorbed or free PAA chains in the system. At relatively low solids loading (20-30 vol%), the yield stress is relatively low (~1 Pa). As solids loading increases above 35 vol%, the yield stress increases dramatically, indicating that there is a change in the way the polymer chains overlap between 30 and 35 vol% solids loadings, most likely due to interparticle distance.

4.3D Storage and loss moduli

As shown in figure 22, the suspensions are all psuedoplastic. Storage modulus and loss modulus can be thought of as components of a suspension that behave more as a solid and a liquid, respectively. The solid component will deform irreversibly under shear, and will store energy, while the liquid component will deform reversibly, dissipating shear. Mathematically, the complex shear modulus, G*, is composed of a real and imaginary component;

$$\tau = G^* \gamma = \left(G' + iG''\right)\gamma \qquad (9)$$

where τ is shear stress, γ is shear strain, and G' and G'' are storage modulus and loss modulus, respectively.[20]

Oscillation tests were performed on suspensions with varying solids loading to determine the storage and loss moduli. The results of these tests are shown in figure 27 for a 20 vol% Al_2O_3 suspension, and in figure 28 for a 40 vol% Al_2O_3 suspension. For

the 20 vol% suspension, both moduli are relatively low. The loss modulus, G", is higher until an angular frequency of about 50 rad/s is reached, at which point storage modulus, G', is higher. This crossover point represents a significant change in the behavior of the suspension. For the 40 vol% suspension in figure 28, the storage modulus is much higher than loss modulus for all angular frequency. Storage and loss moduli are many times greater than for the 20 vol% suspension. The error was also much larger. At this solids loading, the suspension behaves more like a gel than a true liquid.

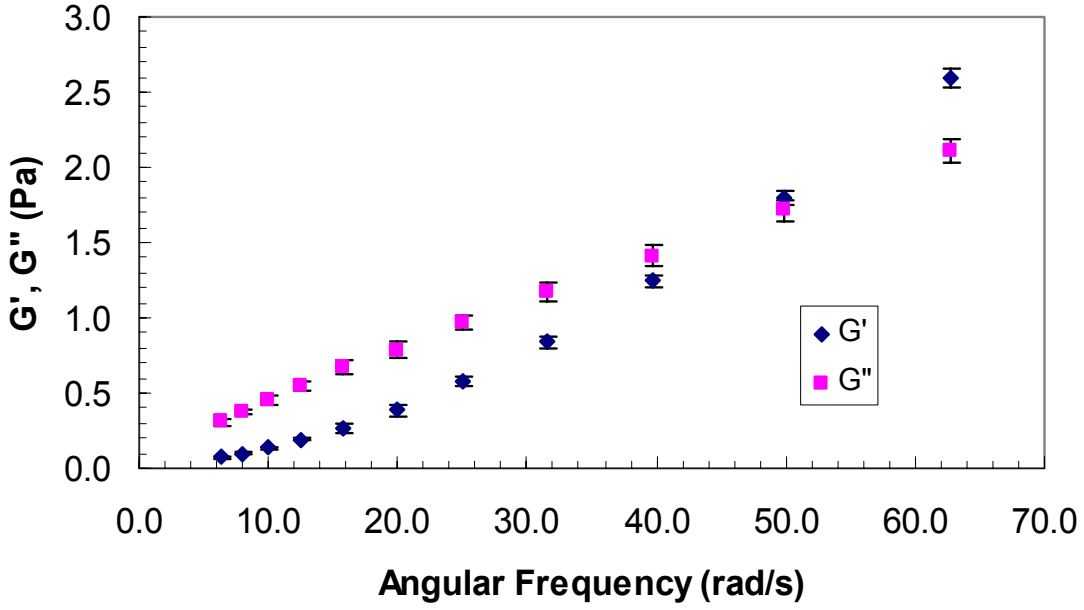

Figure 27. Dynamic moduli at different angular frequencies for a 20 vol% Al_2O_3 suspension.

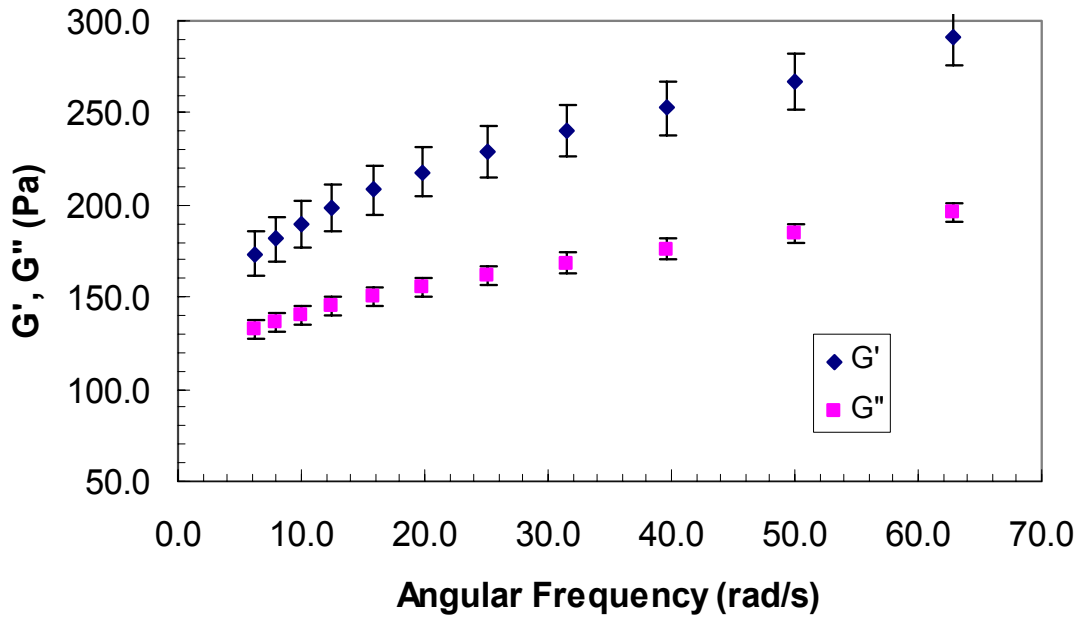

Figure 28. Dynamic moduli at different angular frequencies for a 40 vol% Al_2O_3 suspension.

4.4 Rheology of CNT suspensions

Suspensions containing 40 vol% Al_2O_3 and varying amounts of MWCNT were prepared and tested in equilibrium flow at shear rates from 10/s to 200/s. These data are shown in figures 29 and 30. The suspensions with MWCNT showed a blue coloration, getting darker as more MWCNT was added. In equilibrium flow, suspensions of 0.14 vol% and 0.28 vol% MWCNT actually appeared to decrease the viscosity, though this is in a relatively low-viscosity region. This result is most likely due to error and not a real phenomenon. As figure 30 shows, there appears to be a threshold content of about 1.30 vol%, after which a sharp increase in viscosity can be seen. These results are consistent with previous rheological studies of carbon nanotubes electrostatically dispersed in water,

in which a dramatic change in viscosity was seen beginning at about 0.53 vol% concentration and above.[60,61] There was an order of magnitude difference between the suspension without MWCNT added

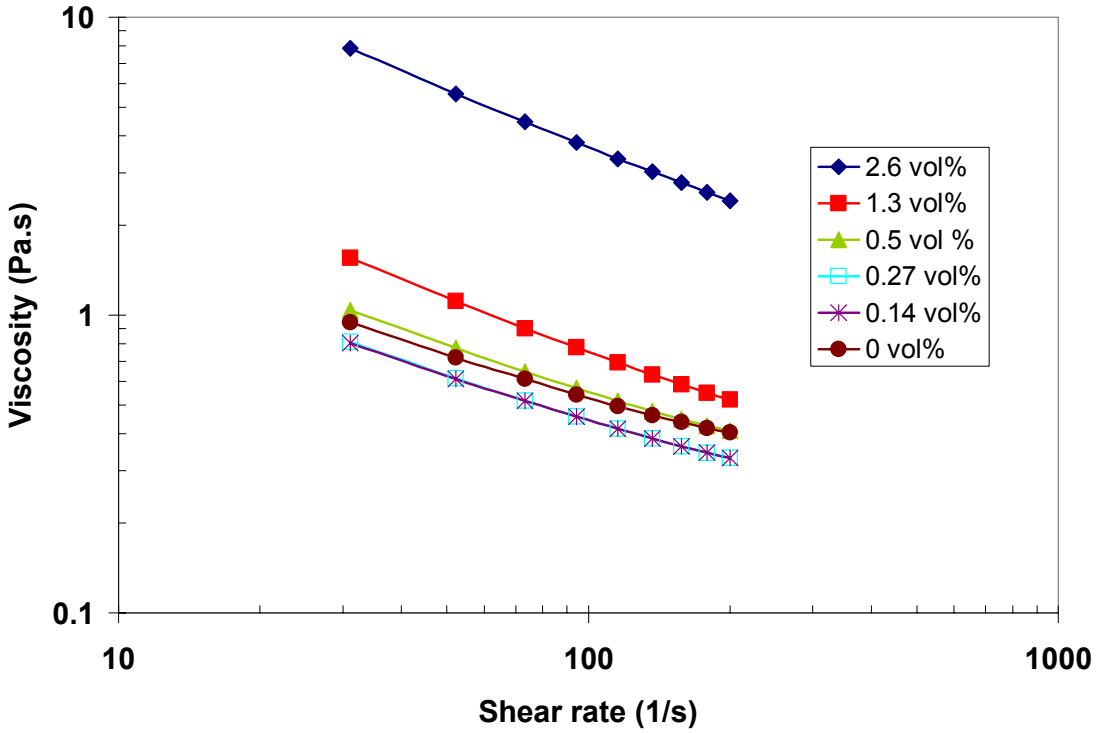

Figure 29. Steady-state flow measurements of 40vol% Al_2O_3 suspensions with varying amounts of MWCNT.

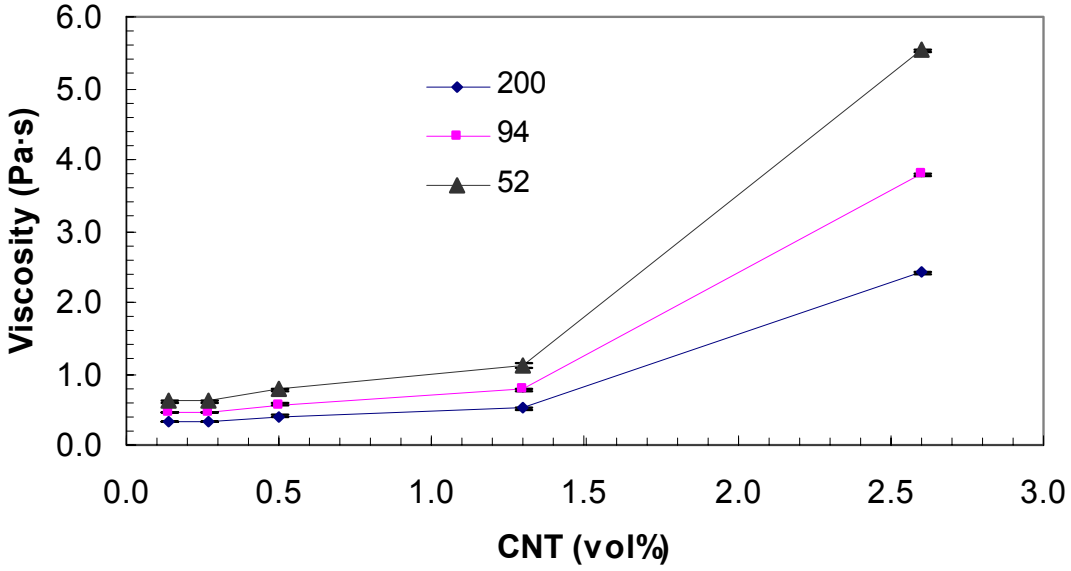

Figure 30. Steady-state flow measurements of 40 vol% Al_2O_3 suspensions with varying amounts of MWCNT at selected shear rates.

and the suspension with 2.60 vol% MWCNT. Equilibrium viscosity increased from 0.56 Pa.s to 0.78 Pa.s with the addition of 1.30 vol% MWCNT, and further increased to 3.79 Pa.s when the MWCNT content was increased to 2.60 vol% (all at shear rate of 94.4/s).

4.5 Freeze casting results

4.5A Mold

To demonstrate the superior surface properties and detail attainable from freeze casting, a suitable mold pattern had to be developed. In this case, a dime was chosen, for its smoothness as well as fine detail. Silicone molds which kept excellent smoothness and surface detail were successfully developed using RTV 664 epoxy. Samples were successfully freeze cast from a suspension of 40 vol% Al_2O_3, 2 wt% PAA, and pH 9.5. Original results showed excellent properties, including a very smooth surface and excellent detail, as seen in figure 31. However, subsequent results showed poorer

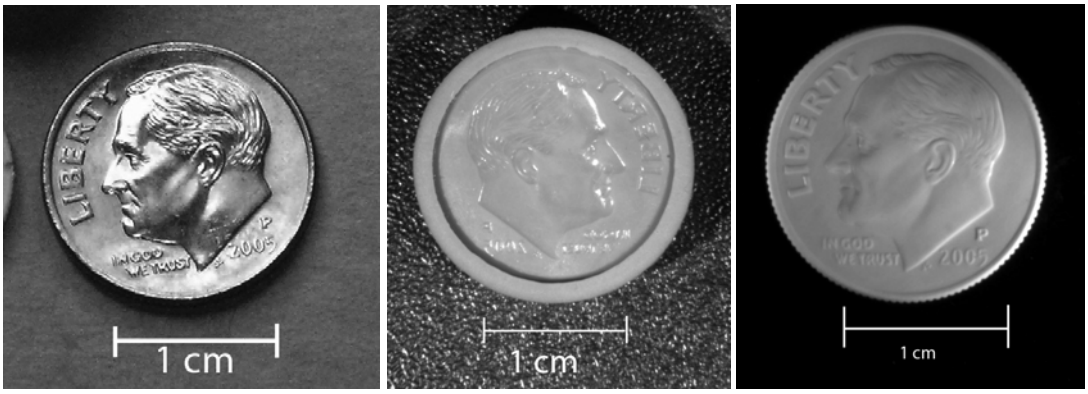

(a) (b) (c)

Figure 31. Photographs of a) metal dime, b) silicone mold made from the dime, and c) freeze cast green Al_2O_3 dime.

characteristics, yielding samples that fell apart easily. It was determined that a resting period is necessary before the samples can be frozen. During this time, the outside of the sample becomes stiff. From visual observation of the sample in the mold, there is considerable shrinkage during this step. This phenomenon was also observed to take place in bottles of the suspension that had been sitting after ball milling was stopped, especially in 40 and 45 vol% Al_2O_3 and 40 vol% Al_2O_3 with 2.60 vol% CNT suspensions.

Obviously, a significant change occurs once the sample is no longer under shear. Several potential causes for this phenomenon were explored. This effect could potentially be due to an interaction of the PAA and glycerol in the suspension, however, the same phenomenon is observed in suspensions prepared without glycerol, and microstructures of green compacts appear similar. Another possible explanation of the stiffening phenomenon is that the shear exerted on the suspension before and during mold filling causes the polymer to align in such a way that facilitates flow, after which the polymer "relaxes." If this relaxation takes place simultaneously with freezing of water

in the system, there is the potential for the PAA to separate from the water, causing an overall weak structure due to inhomogeneous PAA distribution and/or ice crystallization. However, calculations show that relaxation for the polymer used in this system should theoretically take under 1 second,[59] whereas the phenomenon observed in this system occurs in minutes. A more plausible explanation is that the stiffening of the sample is a result of the surface losing moisture, resulting in a higher solids loading, and that the shrinkage is due to air bubbles escaping from the cast suspension. This would explain the higher porosity seen in the samples cast without prerest. The cause of the change in the system during this time is not well understood, and bears further investigation.

Samples of the 40 vol% Al_2O_3 suspension were allowed to relax for a period of one hour in air before the freezing cycle. Green Al_2O_3 discs were freeze cast successfully, and measured using a digital micrometer and an electronic analytical balance. For three green discs, the apparent density was measured to be 55.5, 54.7, and 52.2% of theoretical (for a mixture of 70:30 δ:γ Al_2O_3).

4.5B SEM analysis

Green freeze cast samples were fractured and examined under SEM. The fracture surface was very smooth at the 10 μm range, as shown in figure 32 a). A closer view of the fracture surface shows a relatively porous and homogeneously packed powder compact, suggesting that the suspensions used in freeze casting were well dispersed. Samples freeze cast without the relaxation step were also examined, in figure 32 b). As the image shows, the fracture surface is much rougher, showing features in the tens of microns. These features caused poor resolution in the SEM, as seen in figure 32 b) the

higher resolution image. Unfortunately, a number of very large pores were found internally. These are too large to be caused by poor dispersion, and can only be a result of trapped air in the suspension. Figure 33 shows a relatively large pore caused by an air bubble and a close up side view of the pore, showing the smoothness of the unfractured freeze cast surface. These defects are undesirable because they may significantly lower the strength in the freeze cast samples as well as the fully dense Al_2O_3. In fact, a large crack is visible in figure 33, which propagated directly to the large pore.

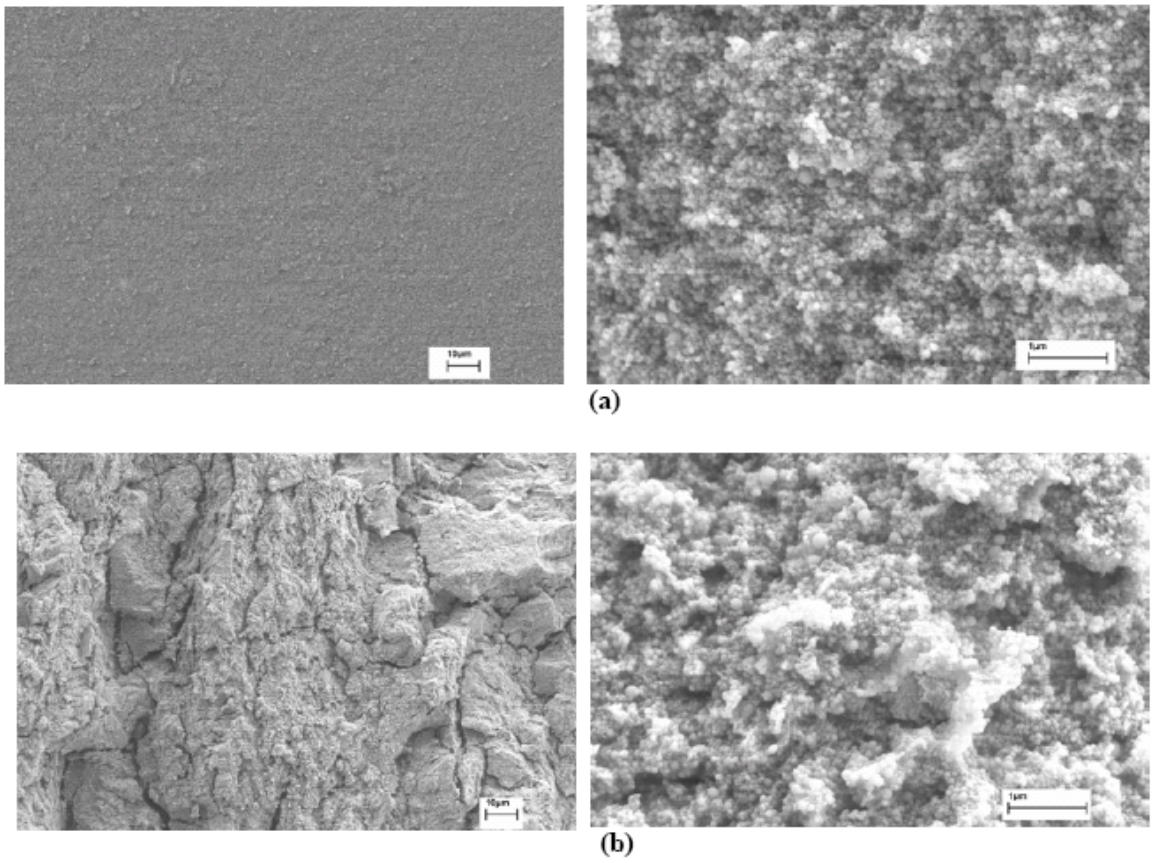

Figure 32. SEM images of fracture surface of freeze cast Al_2O_3 a)with 1 hour prerest before freezing and b) with no prerest before freezing.

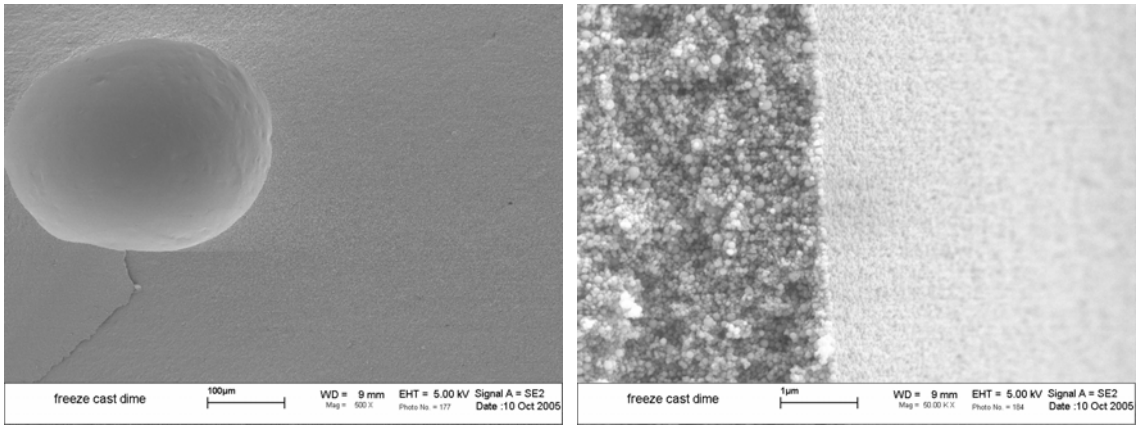

Figure 33. Example of porosity resulting from trapped air bubbles in the powder compact.

4.5C Casting of test specimens

Originally, standard four-point bend test specimens (2 mm x 3 mm) were used to create molds for freeze casting of specimens suitable for strength testing. However, casting of these specimens proved to be problematic. The suspensions of Al_2O_3 nanoparticles showed a strong affinity for the mold wall. This, coupled with the shrinkage during the relaxation step, yielded samples with large shrinkage pipes, unsuitable for bend testing. In order to characterize the bulk strength of the green specimens, an equibiaxial flexural test method was employed. The disc shape was more suited to casting of our suspensions, however, it is suspected that the addition of an appropriate wetting agent into the suspension may significantly reduce the tendency of the suspension to cling to the mold wall, allowing very small overall dimensions to be cast more easily. Disc samples were freeze cast using 40 vol% Al_2O_3 suspensions, and suspensions with 40 vol% Al_2O_3 and 0.14 vol%, 0.28 vol%, 0.53 vol% and 2.6 vol% MWNT.

4.6 Mechanical testing results

Freeze cast Al_2O_3 discs were fractured using the concentric ring test, and the peak load was recorded to determine the strength. All disc samples were broken with the interior (mold-wall) side placed in tensile loading. The samples were examined to ensure that they conformed to a valid fracture mode, per specification. Any samples in which the crack appeared to have initiated outside of the load ring were deemed invalid. For the most part, samples conformed to the medium energy fracture mode. The fracture edges were very smooth, confirming the SEM examinations in section 4.5. Examples of the fractures generated in the green Al_2O_3 discs with varying amounts of MWNT are pictured in figure 34.

After fracture, the sample thickness was measured at the most likely crack initiation point using a digital micrometer. The equibiaxial breaking strength of each sample was calculated via equation (5). Here, the Poisson's ratio, $\boldsymbol{\nu}$ is assumed to be 0.22, a handbook value for fully dense Al_2O_3.[62] While it is not expected that the disc samples will behave similarly to a fully dense Al_2O_3 body, a deviation of ~25% in Poisson's ratio will result in approximately 2% change in σ_f, and the estimate is made with this knowledge. The sample without CNTs showed a higher green strength. Average strength values for the samples can be seen in table 5. It should be noted that because the 2.6wt% MWCNT suspension set into a viscous structure very quickly, it was difficult to create a perfectly flat and smooth surface by freeze casting, and stress raisers may have artificially lowered the strength and caused higher than normal deviation for those samples.

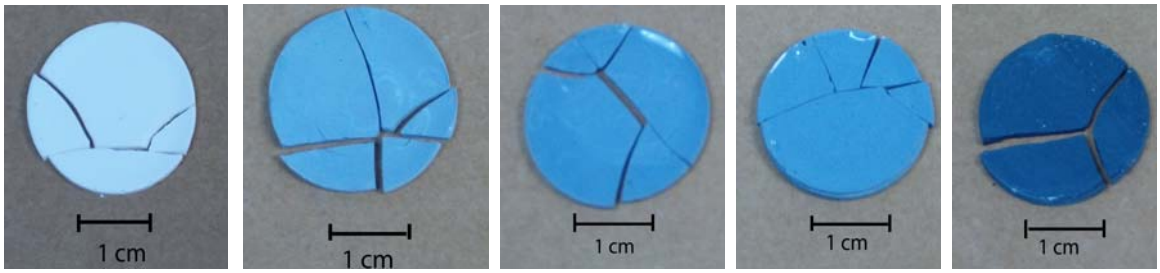

a) b) c) d) e)

Figure 34. Examples of fractures of green MWCNT-Al_2O_3 discs: a) no MWCNT, b) 0.14 vol% MWCNT, c) 0.28 vol% MWCNT, d) 0.53 vol% MWCNT and e) 2.60 vol% MWCNT.

The freeze cast samples with 0.14 vol% MWCNT showed lower equibiaxial strength than pure Al_2O_3, 1.31 MPa compared to 1.62 MPa, while there was an increase in strength from 0.28 to 0.53 vol% MWNT. However, the standard deviations were also very high, and the strength values with deviations overlap between different sample sets. Because of the high deviation and because the sample size is too small at this point, no definitive conclusion about the effect of the presence of CNTs on the strength of the freeze cast samples can be made.

Density was determined using a digital micrometer and analytical balance. In order to calculate relative density, theoretical densities were estimated based on the relative amounts of MWNT and Al_2O_3, and density values of 3.6 g/cm^3 for the Al_2O_3 powder and 1.8 g/cm^3 for the MWCNT. Table 6 shows average apparent density, and calculated theoretical density for green freeze cast Al_2O_3 discs. It should be noted that since the organic contents (PAA and glycerol) were not removed from the discs, the apparent density values were artificially high. The values of apparent density were

normalized to take into account the excess mass of PAA and glycerol in the samples, and the normalized densities were used to calculate relative densities. Normalized apparent density and relative density values for freeze cast MWCNT- Al_2O_3 discs are shown in table 6. Density was high for samples without MWCNT as compared to samples with MWCNT, as was flexural strength. The strength values for different solids loading samples increase with increasing density, however, samples with higher MWCNT content (2.60 vol% suspension) do not follow the trend, possibly because of the rough surface. Figure 35 shows the density and strength data graphically.

Figure 36 shows the strength and density values of green discs without MWCNT and with 0.14 vol% MWCNT. Each data set shows a general trend of higher strength at higher density. For samples with no MWCNT, apparent density varied from about 1.7 g/cm^3 to about 2.4 g/cm^3. For the 0.14 vol% MWCNT samples, apparent density varied from about 1.70 g/cm^3 to about 2.05 g/cm^3. These variations in density could be partially explained by large air bubbles like the ones seen in figure 33. These bubbles make strength and density more difficult to correlate, as the air bubbles could cause lower strength or lower density, or both simultaneously.

Table 5. Strength and standard deviation data for green freeze cast samples.

MWCNT Content (vol%)	Sample Size	Average Flexural Modulus, σ_f (MPa)	Standard Deviation
0	13	1.62	0.37
0.14	14	1.31	0.25
0.28	9	0.92	0.42
0.53	3	1.02	0.21
2.60	4	0.92	0.50

Table 6. Densities of green freeze cast samples.

MWCNT Content (vol%)	Theoretical Density (g/cm^3)	Average Apparent Density (g/cm^3)	Average Apparent Density (Normalized) (g/cm^3)	Average Relative Density (g/cm^3)
0	3.60	1.92	1.83	50.74%
0.14	3.59	1.80	1.71	47.55%
0.27	3.59	1.86	1.77	49.28%
0.53	3.58	1.84	1.74	48.73%
2.60	3.49	1.86	1.76	50.54%

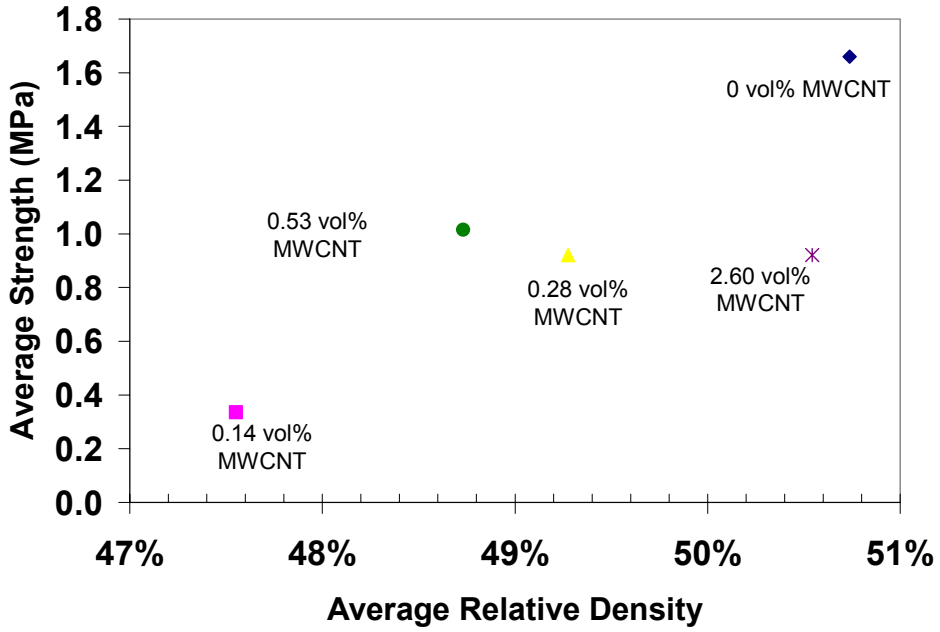

Figure 35. Average density and strength for discs with varying amounts of MWCNT.

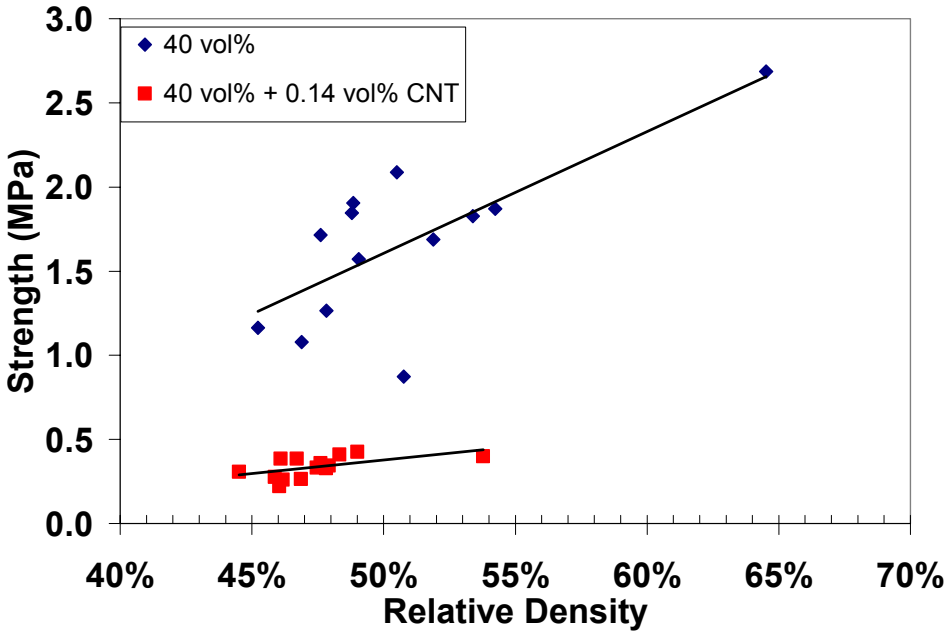

Figure 36. Density and Strength for freeze cast Al_2O_3 discs.

4.7 Sintering results

Samples of freeze cast Al_2O_3 were weighed and debinded in air to determine the effectiveness of the process. For the 40 vol% Al_2O_3 freeze cast sample, approximately 5.3 wt% organics (glycerol and PAA) should be present. Heating the sample to 450°C for two hours in air was successful at removing over 4% of the overall weight of the sample. Previous work had determined that the addition of glycerol will leave residue in the sample even after debinding.

For comparison purposes, a pure Al_2O_3 freeze cast sample was debinded and heated in air at a rate of 40°C/min to 1500°C, then held for 6 hours. SEM images of the mold face surface and fracture surface of that sample are shown in figures 37 and 38. Although the grains are micron-sized, the sample did not achieve full density. The grains are interconnected and multifaceted, indicating grain coarsening was in effect.

Freeze cast samples were debinded, and densified in the two-step profile in section 3.8. After completion of the heating run, the sample was broken with a hammer and coated with gold for SEM analysis. Figures 39 and 40 show the microstructure of the Al_2O_3 sample. Although the grains appear to be submicron-sized, the density is relatively low, and there are many pores. The powder particles have formed a continuous network. The heating profile was not sufficient to fully densify the green sample; however, it may be possible to achieve full density by heating the sample to 1500°C, then cooling to 1265°C and holding that temperature for longer than ten hours.

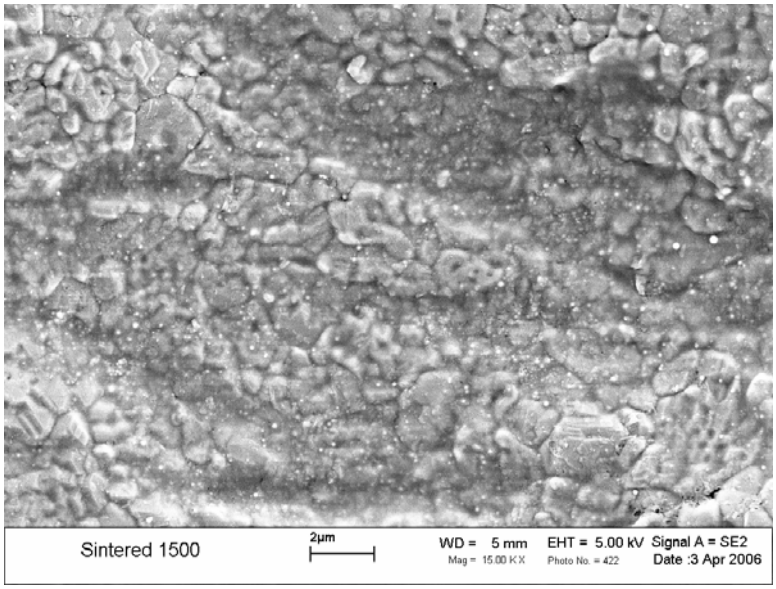

Figure 37. Free surface of a freeze cast Al_2O_3 sample after heating at 1500 for 6 hours.

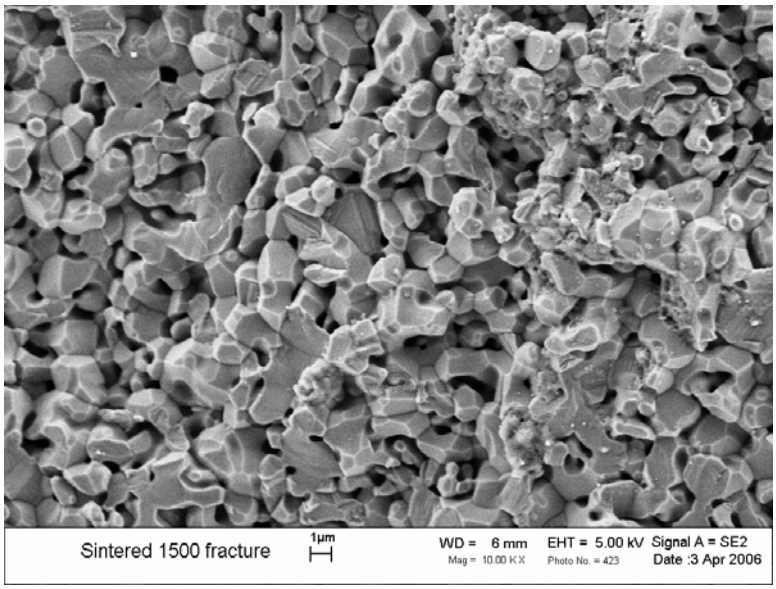

Figure 38. Fracture surface of a freeze cast Al_2O_3 sample after heating at 1500 for 6 hours.

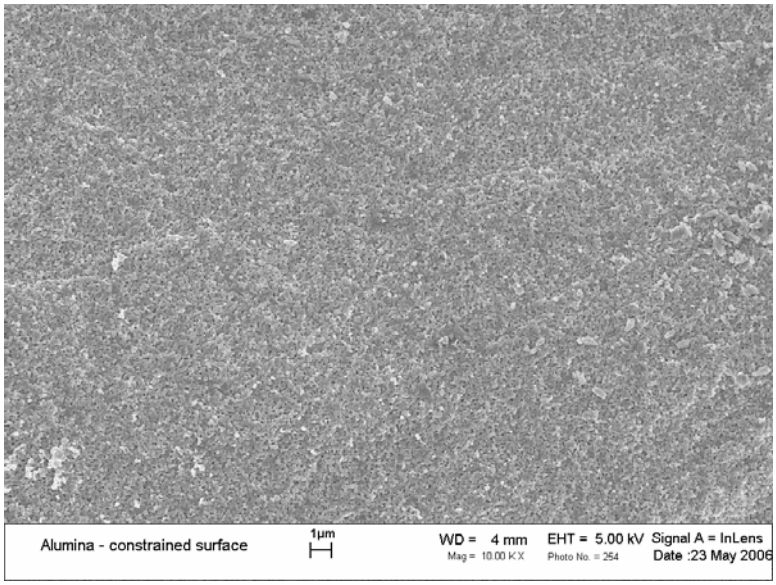

Figure 39. Scanning Electron Micrograph of the surface of Al_2O_3 sample after two-step heating.

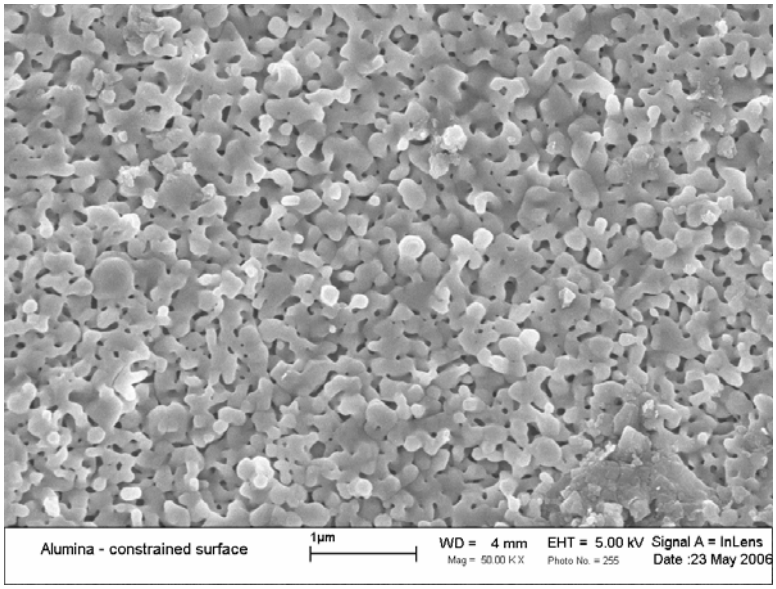

Figure 40. Scanning Electron Micrograph of the surface of Al_2O_3 sample after two-step heating.

Chapter 5. Summary

A procedure for making MWCNT- Al_2O_3 suspensions was developed. As-received Al_2O_3 powder was consistent with the vendor's data. Zeta potential data indicated that the adsorbed PAA and PMAA were effective dispersants. Aqueous suspensions were prepared using nanoparticulate Al_2O_3 with a carboxylic acid dispersant. PAA with M_w = 1800 was deemed to be a better dispersant than PMAA with M_w=15,000 based on adsorption and rheology testing.

By measuring the effect of different parameters on the adsorption of polymer and viscosity of nanoparticle suspensions, the optimum values for the system were determined to be 40 vol% Al_2O_3, 2.00 wt% PAA, and pH 9.5. PAA adsorption reaches a plateau of >30 mg/m^2 after 2 wt% (of Al_2O_3) PAA is added. Though more polymer was adsorbed at lower pH, viscosity data were better at high pH, indicating the importance of configuration of the adsorbed polymer with regard to stabilization.

All suspensions were shown to be shear-thinning, with a two orders of magnitude increase in viscosity when solids loading increases from 20 to 40 vol% Al_2O_3. The maximum solids loading was predicted (based on measured data) to be 50.7 vol%. The Al_2O_3 suspensions conformed to the Herschel-Bulkley rheology model.

Suspensions were prepared with MWCNT and 40 vol% Al_2O_3. Small additions (<0.5 vol%) of MWCNT did not strongly affect the flowability of 40 vol% Al_2O_3 suspensions, but the addition of 2.6 vol% MWCNT caused an order of magnitude increase in the viscosity. Evidence was seen of a critical level of MWCNT in the suspension after which the behavior was different.

Suspensions of 40 vol% Al_2O_3 were successfully freeze cast, and visually, showed excellent surface smoothness and detail from the mold. A unique phenomenon was discovered upon freezing the 40 vol% Al_2O_3 suspension, requiring a relaxation step before cooling of the sample began. Samples that were freeze cast without relaxation crumbled or delaminated when being handled. SEM images show a much rougher fracture surface for samples that had not been relaxed, and a non-homogeneous microstructure.

Freeze cast disc specimens with and without MWCNT were broken in a concentric ring apparatus to measure flexural strength. The samples without CNT showed the highest strength at 1.62 MPa, but a higher standard deviation than the samples with 0.14 vol% MWCNT. There was seen a trend of increasing strength with increasing density for individual conditions, however, that trend did not extend over all CNT conditions, in part due to the inability of making regular samples with the 0.5 and 2.3 vol% CNT suspensions. No statement could be made about the effect of different amounts of MWCNT in Al_2O_3 suspensions based on the data.

Preliminary work was performed to investigate a densification procedure. The freeze cast sample was heated to 1500°C and held for 6 hours. This procedure was not effective in preventing grain growth or in fully densifying the green sample. Another sample was heated to 1500 and cooled immediately to 1265°C and held, which was also ineffective, but yielded much more promising results.

Chapter 6. Future Work

The dispersion of the system with glycerol and PAA additives has been investigated, but there are other additives that might be of interest, specifically surfactants and anti-foaming agents. The addition of 0.25 wt% surfactant has been shown to be beneficial in other work as a wetting agent[48,49], although excellent surface detail was achieved without one. Additionally, it was noted that one of the main difficulties in processing the suspension was dissolved or trapped air in the suspensions, which become visible pores in the freeze dried parts. Some method of removing the trapped air, either by an anti-foam agent or by some mechanical means, is clearly needed.

Sun and Gao showed that it is possible to successfully coat the surface of carbon nanotubes with ceramic nanoparticles. By coating the surface of the CNT with oxide particles, the CNTs can be more easily dispersed through the system. In this work, the CNTs were merely added to the existing Al_2O_3 suspension. By performing a prior CNT separation and heterocoagulation procedure, the composite suspension might exhibit greatly reduced viscosity.

A greater sample set is desirable to analyze strength data. Although some interesting trends were seen, the sample sets were very small. Removal of the air bubbles may lead to a stronger correlation between density and strength in green samples.

Further work should be done to densify the green compacts. Although the work was unsuccessful in creating a fully dense microstructure, the images show that the sample could possibly become fully dense if the sample was held at 1265°C for a longer period of time. Additionally, it will be important to see what effect, if any, the inclusion of the carbon nanotubes has on grain size and densification. It may be advantageous to

eliminate large porosity, so that trapped oxygen will not react with the CNTs at high temperature.

Fully dense samples of the MWCNT-Al_2O_3 composite should be tested using the equibiaxial flexural test apparatus. The correlation between amount of MWCNT in the sample and strength (if any) should be examined.

References

[1] M. J. Mayo, "Processing of nanocrystalline ceramics from ultrafine powders," International Materials Reviews 41 [3] 89-112 (1996).

[2] S. Iijima, "Helical Microtubules of Graphitic Carbon," *Nature* **354** 56-58 (1991).

[3] M. S. Dresselhaus, G. Dresselhaus, and P. Eklund, *Science of Fullerenes and Carbon Nanotubes*, Academic Press, New York, 1996.

[4] A. N. Goldstein, *Handbook of Nanophase Materials*, Marcel Dekker, Inc., New York, 1997.

[5] A. G. Rinzler, J.H. Hafner, P. Nikolaev, L. Lou, S.G. Kim, D. Tomanek, P. Nordlander, D.T. Colbert and R. E. Smalley, "Unraveling Nanotubes: Field Emission from an Atomic Wire," *Science* **269** [5230] 1550-1553 (1995).

[6] W. A. de Heer, W. S. Bacsa, A. Chatelain, T. Gerfin, R. Humphrey-Baker, D. Ugarte and L. Forro, "Aligned Carbon Nanotube Films: Production and Optical and Electronic Properties," *Science* **268** [5212] 845-847 (1995).

[7] P. M. Ajayan and Sumio Iijima, "Capillarity-Induced Filling of Carbon Nanotubes," *Nature* **361** [6410] 333-334 (1993).

[8] R. S. Ruoff, J. Tersoff, D. C. Lorents, S. Subramoney, and B. Chan, "Radial Deformation of Carbon Nanotubes by van der Waals Forces," *Nature*, **364** 514-516 (1993).

[9] M.-F. Yu, B. S. Files, S. Arepalli, and R. S. Ruoff, "Tensile Loading of Ropes of SingleWall Carbon Nanotubes and their Mechanical Properties," *Phys. Rev. Lett*., **84** 5552-5555 (2000).

[10] L. Dai, A. Patil, X. Gong, Z Guo, L. Liu, Y. Liu, and D. Zhu, "Aligned Nanotubes," *ChemPhysChem*, **4** [11] 1150-1169, 2003.

[11] Z. Jia, Z. Wang, C. Xu, J. Liang, B. Wei, D. Wu, S. Zhu, "Study on Poly(Methyl Methacrylate)/Carbon Nanotube Composites," *Mat. Sci. Eng*. **A271** 395–400 (1999).

[12] S. J. Park, M. S. Cho, S. T. Lim, H. J. Choi,* M. S. Jhon, "Synthesis and Dispersion Characteristics of Multi-Walled Carbon Nanotube Composites with Poly(methyl methacrylate) Prepared by In-Situ Bulk Polymerization," *Macromol. Rapid Commun*., **24** 1070–1073 (2003).

[13]D. Colbert, "Single-Wall Nanotubes: A New Option for Conductive Plastics and Engineering Polymers," *Plastics Additives & Compounding* **5** [1] 18-25 (2003).

[14] M. J. Mayo, "Nanoceramic Toys," *Advanced Engineering Materials*, **2** [7] 409-415 (2000).

[15] G. W. Scherer, "Theory of Drying," *J. Am. Ceram. Soc*, **73** [1] 3-14 (1990).

[16] F. London, *Z. Phys* 89, 736 (1934).

[17] D. Napper, *Polymeric Stabilization of Colloidal Dispersions*; pp 4-7. Academic Press, London, 1983.

[18] J. Cesarano III and I. A. Aksay, "Processing of Highly Concentrated Aqueaous α-Alumina Suspensions Stabilized with Polyelectrolytes," *J Am Ceram Soc*, **71** [12] 1062-1067 (1988)

[19] H. Stein, *The Preparation of Dispersions in Liquids*; pp 15-34. Marcel Dekker, New York, 1995.

[20] J. Lewis, "Colloidal Processing of Ceramics," *J Am Ceram Soc*, 83 [10] 2341-2359 (2000).

[21] J. Cesarano III, I. A. Aksay, and A. Bleier, "Stability of Aqueous α - Al_2O_3 Suspensions with Poly(methacrylic acid) Polyelectrolyte," *J Am Ceram Soc*, **71** [4] 250-255 (1988)

[22] W. Sigmund, N. Bell, and L. Bergstrom, "Novel Powder-Processing Methods for Advanced Ceramics," *J Am Ceram Soc*, 83 [7] 1557-1574 (2000).

[23] B. Singh, S. Bhattacharjee, L. Besra and D. K. Sengupta, *Ceramics International*, **30** [6] 939-946 (2004).

[24] J. Cho, and F. Dogan, "Colloidal Processing of Lead Lanthanum Zirconate Titanate Ceramics," *J Mat Sci*, **36,** 2397-2403 (2001).

[25] H. A. van der Schee and J. Lyklema, "A Lattice Theory of Polyeletrolyte Adsorption," *J Phys. Chem.,* 88 [26] 6661-6667 (1984).

[26] M. N. Rahaman, *Ceramic Processing and Sintering*, second edition, Marcel Dekker, New York, 2003, pp. 227-247, pp. 330-344.

[27] D. R. Dinger, *Rheology for Ceramists*, pp. 1-22, Dinger Ceramic Consulting Services, Clemson, SC, 2002.

[28] J. S. Reed, *Principles of Ceramics Processing*, Second Edition, pp.277-309, Wiley, New York, 1995.

[29] I M Krieger and M Dougherty, "A Mechanism for Non-Newtonian Flow in Suspensions of Rigid Spheres," *Trans. Soc. Rheol.* **3** 137-152 (1959).

[30] D. Liu, "Particle packing and rheological property of highly-concentrated ceramic suspensions: Φm determination and viscosity prediction" *J Mat Sci* **35** 5503-5507 (2000).

[31] C. E. Huggins, "Blood Freezing," in S. A Goldblith, L. Rey, and W. W. Rothmayr, eds., *Freeze Drying and Advanced Food Technology*, pp. 51-60, Academic Press, New York, 1975.

[32]J. Laurie, C. M. Bagnall, B. Harris, R. W. Jones, R. G. Cooke, R. S. Russell-Floyd, T. H. Wang, and F. W. Hammett, "Colloidal Suspensions for the Preparation of Ceramics by a Freeze Casting Route," Journal of Non-Crystalline Solids, **147**, 320-325 (1992).

[33] M. J. Statham, F. Hammett, B. Harris, R. G. Cooke, R. M. Jordan, and A. Roche, "Net-Shape Manufacture of Low-Cost Ceramic Shapes by Freeze-Gelation," *Journal of Sol-Gel Science and Technology* **13**. 171-175 (1998).

[34] C. E. Huggins, "Prevention of Hemolysis of Large Volumes of Red Blood Cells Slowly Frozen and Thawed in the Presence of Dimethylsulfoxide," *Transfusion* **3** 483 (1963).

[35]C. Laurent, A. Peigney, O. Dumortier, and A. Rousset, "Carbon Nanotubes-Fe-Alumina Nanocomposites. Part II: Microstructure and Mechanical Properties of the Hot-Pressed Composites," *J. Euro. Ceram. Soc*., 18 2005-2013 (1998).

[36] E. Flahaut, A. Peigney, Ch. Laurent, C. Marliere, E. Chastel, and A. Rousset, "Carbon Nanotubes-Metal-Oxide Nanocomposites: Microstructure, Electrical Conductivity, and Mechanical Properties," *Acta Mater*., 48 3803-3812 (2000).

[37] A. Peigney, Ch. Laurent, E. Flahaut, and A. Rousset, "Carbon Nanotubes in Novel Ceramic Matrix Nanocomposites," Ceram. Inter., 26 677-683 (2000).

[38] G.-D. Dong Zhan and A. K.. Mukherjee, "Carbon Nanotube Reinforced Alumina-Based Ceramics with Novel Mechanical, Electrical, and Thermal Properties," *Int. J. Appl. Ceram. Technol*., **1** [2] 161-71 (2004).

[39] J. Sun and L. Gao, "Development of a Dispersion Process for Carbon Nanotubes in Ceramic Matrix by Heterocoagulation, *Carbon* **41** 1063-1068 (2003).

[40] J. L. Bahr, and J. M. Tour, "Covalent Chemistry of Single-wall Carbon Nanotubes," *J. Mater. Chem*., **12** 1952-1958 (2002).

[41] V. C. Moore, M. S. Strano, E. H. Haroz, R. H. Hauge, and R. E. Smalley, "Individually Suspended Single-Walled Carbon Nanotubes in Various Surfactants" *Nano Letters* **3** [10] 1379-1382 (2003).

[42] J.-M. Bonard, *Adv. Mater*. **9** 827 (1997).

[43] C. Richard, F. Balavoine, P. Schultz, T. Ebbesen, and C. Mioskowski, "Supramolecular Self-Assembly of Lipid Derivatives on Carbon Nanotubes," Science 300 775-778 (2003)

[44] L. Jiang, L. Gao, and J. Sun, "Production of aqueous colloidal dispersions of carbon nanotubes," *Journal of Colloid and Interface Science* 260 89–94 (2003).

[45] J. Fan, D. Zhao, M. Wu, Z. Xu, and J. Song, "Preparation and Microstructure of Multi-Wall Carbon Nanotubes-Toughened Al_2O_3 Composite," *J. Am. Ceram. Soc*., **89** [2] 750–753 (2006).

[46] Q. Huang and L. Gao, "Manufacture and Electrical Properties of Multiwalled Carbon Nanotube/$BaTiO_3$ Nanocomposite Ceramics.

[47] D. Koch, L. Andresen, T. Schmedders and G. Grathwohl, "Evolution of Porosity by Freeze Casting and Sintering of Sol-Gel Derived Ceramics," *Journal of Sol-Gel Science and Technology*, **26** 149-152 (2003).

[48] S. W. Sofie and F. Dogan, "Freeze Casting of Aqueous Slurries with Glycerol" *J Am Ceram Soc* **84** [7] 1459-1464 (2001).

[49] F. Dogan and S. W. Sofie, "Microstructural Control of Complex-Shaped Ceramics Processed by Freeze Casting," *Cermics Forum Int.,* **79** [5] E35-E38 (2002).

[50] C. S. Miner and N. N. Dalton, *Glycerol*, pp. 270-284, Reinhold, New York, 1953.

[51] V. F. Petrenko, "Structure of Ordinary Ice I_h, Part I: Ideal Structure of Ice," Report No. 93–25, U.S. Army Corps of Engineers, Cold Regions Research and Engineering Laboratory, Hanover, NH, 1993.

[52] R. Arnold and J. T. G. Overbeek, "The Dissociation and Specific Viscosity of Polymethacrylic Acid," *Rec. J. R. Nefh. Chem. Soc.,* **69**, 192-206 (1950).

[53] Y. Q. Liu and L. A. Gao, "Dispersion of Aqueous Alumina Suspensions Using Copolymers with Synergistic Functional Groups," *Mater. Chem. Phys*., **82**[2]362-9 (2003).

[54] ASTM Designation C 1499-06, "Standard Test Method for Monotonic Equibiaxial Flexural Strength of Advanced Ceramics at Ambient Temperature," American Society for Testing and Materials International, West Conshocken, PA, 2006.

[55] ASTM Designation C1161-02c, "Standard Test Method for Flexural Strength of Advanced Ceramics at Ambient Temperature," American Society for Testing and Materials International, West Conshocken, PA, 2002.

[56] U. Soltesz, H. Richter, and R. Kienzler, "The Concentric-Ring Test and its Application for Determining the Surface Strength of Ceramics," in *Ceramics in Clinical Applications* (*High Tech Ceramics*) pp. 149-158, Elsevier, Amsterdam 1987.

[57] D. R. Lide, ed., *CRC Handbook of Chemistry and Physics*, 72nd Edition, pp. 9-2-9-15, CRC Press, Boston, MA 1991-1992.

[58] H. Guldberg-Pedersen and L. Bergstrom, "Stabilizing Ceramic Suspensions Using Anionic Polyelectrolytes: Adsorption Kinetics and Interparticle Forces," *Acta Materialia* **48** 4563-4570 (2000).

[59] K. Lu, C. S. Kessler, and R. M. Davis, "Optimization of a Nanoparticle Suspension for Freeze Casting," *J. Am. Ceram. Soc*., accepted.

[60] M. S. P. Shaffer and A. H. Windle, "Analogies between Polymer Solutions and Carbon Nanotube Dispersions," *Macromolecules*, **32**, 6864-6866 (1999).

[61] I. A. Kinloch, S. A. Roberts and A. H. Windle, "A Rheological Study of Concentrated Aqueous Nanotube Dispersions, *Polymer* **43**, 7483–7491 (2002).

[62] N. Dowling, *Mechanical Behavior of Materials*, second edition p. 178, Prentice-Hall, Upper Saddle River, New Jersey 1999.

VITA

Christopher Steven Kessler was born December 17, 1979 in Richmond, Virginia, where he grew up. In 1998 Chris graduated from The Governor's School for Government and International Studies. From 2001-2002 he worked at ITT Industries Night Vision in Roanoke as a member of the co-operative education program. In addition to participating in several research projects for the MSE department, Chris was an active member of Tau Beta Pi and Kappa Theta Epsilon honor societies in his undergraduate career. After earning his bachelor's degree from the Materials Science and Engineering Department in 2004, Chris began work on his M.S. In his graduate career Chris has been credited as co-author for several published papers, and worked on an additional project studying nanotechnology and diversity.